Journal of Superconductivity and Novel Magnetism
https://doi.org/10.1007/s10948-023-06608-2

ORIGINAL PAPER

Developing a Concept of an Effective Field in the Intergrain Medium of a Granular Superconductor: Effect of the Intragrain Meissner Currents and Abrikosov Vortices Trapped in Grains on the Magnetotransport Properties of a Y-Ba-Cu-O Granular HTS

D. A. Balaev[1] · S. V. Semenov[1] · D. M. Gokhfeld[1]

Received: 7 February 2023 / Accepted: 3 August 2023

Abstract
Granular high-temperature superconductors (HTSs) are characterized by the hysteretic field dependences of magnetoresistance R(H) and critical current I_C(H). These hysteretic effects are described within the concept of an effective field in the intergrain medium. The effective field is a superposition of external magnetic field H and the field induced by the magnetic moments of superconducting grains into intergrain spacings (grain boundaries). The magnetization of superconducting grains is determined by two contributions: Meissner (shielding) currents (**MC**) and trapped magnetic fluxes (Abrikosov vortices (**AV**)). To develop the concept of an effective field in the intergrain medium, the magnetotransport properties (R and I_C) have been compared for two cases: (**AV**) the magnetization of superconducting grains is only determined by the trapped magnetic flux (zero external field) and (**MC**) HTS grains are in the Meissner state (the external field is weaker than the first critical field of grains). In a set of experiments, the main features of the hysteretic R(H) and M(H) dependences have been illustrated and the external conditions for implementing the **AV** and **MC** states have been established. It has been found that the effects of the Abrikosov vortices and intragrain Meissner currents on an effective field in the intergrain medium at the same magnetization values are noticeably different. This is a nontrivial fact that requires a thorough study of the impact of the anisotropy of the superconducting properties of grains on the configuration of the Meissner currents in them, as well as on the orientation of vortices both inside grains and near their surface. We suggest the explanation of observed stronger effect of the Meissner currents on the intergrain medium as compared with the effect of the Abrikosov vortices.

Keywords Granular HTS · Effective field in the intergrain medium · Magnetoresistance hysteresis · Magnetization hysteresis · Trapped flux · Meissner current · Abrikosov vortex

1 Introduction

1.1 Effective Field in the Intergrain Medium of a Granular Superconductor

Study of the magnetotransport properties of a superconducting material is important for both its characterization and understanding the mechanisms of pinning of the Abrikosov vortices and related dissipation processes (the occurrence of nonzero resistance) in an external field. On the one hand, in classical high-temperature superconductor (HTS) systems, e.g., in yttrium, bismuth, and lanthanum ones, many features of the magnetic phase diagrams, in particular, vortex lattice state − magnetic field and vortex lattice state − temperature, were determined quite a long time ago [1–5]. On the other hand, the above applies to single-crystal (bulk or film) systems, whereas in polycrystalline (hereinafter referred to as granular) HTS materials, the physical mechanisms of dissipation are more complex. Here, the crucial factor is the presence of grain boundaries, which determine the critical current of a bulk granular HTS. The thickness of grain boundary d is no thicker than few nanometers. In conventional low-temperature superconductors, such a size barely

✉ D. M. Gokhfeld
gokhfeld@iph.krasn.ru

[1] Kirensky Institute of Physics, Krasnoyarsk Scientific Center, Siberian Branch, Russian Academy of Sciences, Krasnoyarsk 660036, Russia

Published online: 22 August 2023

affects the dissipation, because the inequality $\xi >> d$ (ξ is the coherence length) is strictly valid, while in the HTSs with a very small ξ value, the equation $\xi \sim d$ is legitimate. In the latter case, transport of the superconducting current between two neighboring grains occurs by means of the Josephson effect. Then, the term "two-level superconducting system" [6] can be applied to a granular superconductor in which HTS grains are characterized by the strong superconductivity and the subsystem of grain boundaries is a weak superconductor, according to the weak superconductivity term [7] commonly used for superconducting weak links or Josephson junctions.

The presence of grain boundaries is not the only factor complicating the pattern of dissipation in granular HTSs in an external magnetic field. Each superconducting grain induces its own magnetic response $\mathbf{M}_G$ to the external field; as a result, the subsystem of grain boundaries is no longer in the external field, but in some effective field $\mathbf{B}_{eff}$. This effective field is a superposition of the external field $\mathbf{H}$ and the field induced by the magnetic moments of HTS grains [8–12] (see Fig. 1). Here, there is a direct analogy with the Weiss molecular field in ferro- and ferrimagnets. It is clear that, similarly to the Weiss molecular field, the field induced in the intergrain medium of a granular superconductor should be related to magnetizations M_G of individual grains and magnetization M of the entire superconductor. Therefore, in the spacing between two neighboring grains, we have

$$\mathbf{B}_{eff}(\mathbf{H}) = \mathbf{H} + \alpha_1 \cdot 4\pi \cdot \mathbf{M}_{G1}(\mathbf{H}) + \alpha_2 \cdot 4\pi \cdot \mathbf{M}_{G2}(\mathbf{H}). \quad (1)$$

Here, α_1 and α_2 include the demagnetizing grain shape factor and the effect of the magnetic flux compression in the intergrain medium (see Fig. 1). The latter effect is caused by incomparably different grain sizes (by several micrometers and more) and grain boundary thicknesses (few nanometers or less). Equation (1) is written in the vector representation. To pass to the scalar form, it makes sense to consider the mutual direction of $\mathbf{M}_G$ and external field $\mathbf{H}$ ($\mathbf{H} \parallel \mathbf{Z}$). In the increasing external field $H = H_{inc}$, the $\mathbf{M}_G$ projection onto the $\mathbf{Z}$ axis is negative (diamagnetism), while in the decreasing field $H = H_{dec}$, it is positive (the trapped flux effect), which is illustrated in Fig. 1. Hence, the $\mathbf{B}_{eff}$ projection onto the $\mathbf{Z}$ axis is $B_{effZ}(H) = H - \alpha_1 \cdot 4\pi \cdot M_{G1}(H) - \alpha_2 \cdot 4\pi \cdot M_{G2}(H)$. Averaging the effective field over all grain boundaries in a sample consisting of a great number of grains, at $\mathbf{M} = \Sigma\mathbf{M}_{Gi}$, we can write

$$B_{eff}(H) = |H - \alpha \cdot 4\pi \cdot M(H)|. \quad (2)$$

The absolute value is taken in Eq. (2) since, in the dissipation processes (microcurrents I_{micro} in Fig. 1), the value, rather than the direction, of the effective field (parallel of antiparallel to the $\mathbf{Z}$ axis) is important and the parameter α characterizes now the effective magnetic flux compression in the intergrain medium [13–18] for the entire sample (the superconducting material).

The described concept of an effective field in the intergrain medium of a granular superconductor made it possible to explain most of the experimental features of the magnetotransport properties of granular HTSs: the shape and nature of the field dependences of the magnetoresistance R(H) [13–18], relaxation of the resistance under certain conditions (at H = const and T = const) [11, 13], magnetoresistance anisotropy in external field $\mathbf{H}$ applied perpendicular or parallel to the macroscopic transport current direction [19–22], and effect of the thermomagnetic prehistory on the R(T) dependences [22–24]. Importantly, Eq. (2) only describes the value of the total field in the intergrain

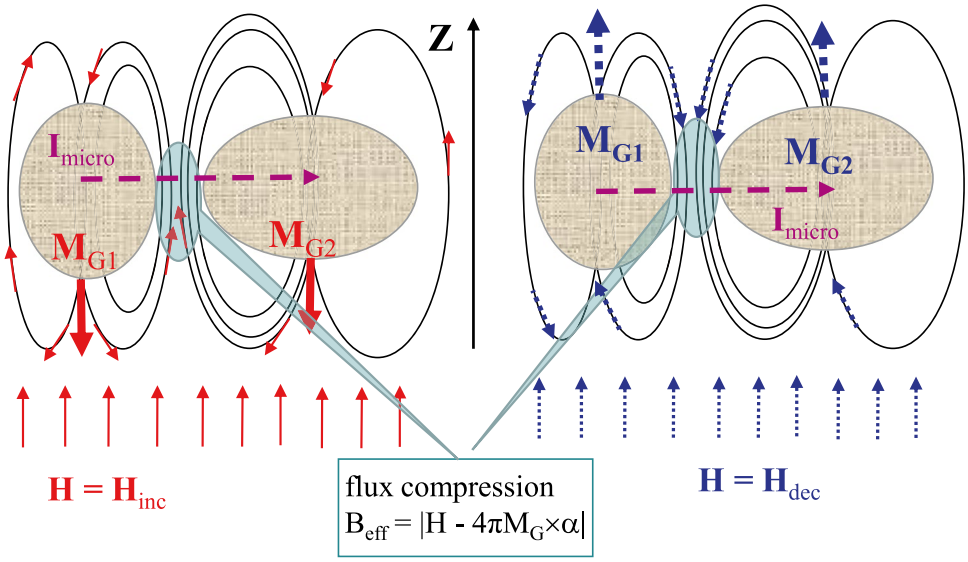

Fig. 1 Schematic of mutual directions of external field $\mathbf{H}$ ($\mathbf{H} \parallel \mathbf{Z}$), magnetic moments $\mathbf{M}_{G1}$ and $\mathbf{M}_{G2}$ of two neighboring HTS grains (ovals), and magnetic induction lines from $\mathbf{M}_{G1}$ and $\mathbf{M}_{G2}$ in the increasing external field $\mathbf{H} = \mathbf{H}_{inc}$ (on the left) and decreasing external field $\mathbf{H} = \mathbf{H}_{dec}$ (on the right). The space between grains is a grain boundary, through which superconducting carriers (microcurrents $\mathbf{I}_{micro}$) tunnel. In the grain boundaries with a thickness of several nanometers or thinner, the magnetic flux is compressed

medium, while the magnetoresistance is already a function not of the external field H, but of the effective field B_{eff}: $R(H) = R(B_{eff}(H))$ or $R = f(B_{eff})$. In the theories of the dissipation in type-II superconductors, f is the Arrhenius function: $R(H) \sim \exp(-U_P(H, T, j) / k_B T)$, where $U_P(H, T, j)$ is the dependence of the pinning potential on the transport current density, temperature, and external field [1, 25]. As applied to granular HTSs, instead of U_P, the Josephson energy E_J of the coupling between grains is used; then, the magnetoresistance will be a function of the effective field B_{eff}: $R(H) \sim \exp(-E_J(B_{eff}, T, j) / k_B T)$ [22, 24, 26, 27].

We note that study of the magnetotransport properties of synthesized bulk superconductors is an integral part of their characterization [28–43]. In this regard, further development of the concept of an effective field in the intergrain medium is important for understanding the mechanisms responsible for the magnetotransport characteristics of new materials. In [44], a targeted search was suggested for the hysteretic effects in the behavior of the magnetoresistance of hydride superconductors, which exhibit superconductivity under high pressures up to near-room temperature [42, 43].

1.2 Formulation of the Problem and Structure of the Article

Now, the main nontrivial fact in describing the magnetotransport properties of granular HTSs using Eq. (2) is the interplay between the magnetization of HTS grains and the effective field in intergrain spacings. Hence, any peculiarity in the magnetic hysteresis loop must find its correspondence with the nature of the magnetoresistance. To further develop the concept of an effective field in the intergrain medium, in the present work we explore the behavior of the magnetoresistance in the two special cases: (**MC**) the magnetization of grains is only determined by the Meissner effect (the external field has such a value that the flux is not trapped into grains yet) and (**AV**) the magnetization of grains is only determined by the Abrikosov vortices (there is no external field, there are no Meissner currents, and the flux is trapped into grains). Do these extreme cases have the same effect on the effective field on the intergrain medium? We have performed the detailed investigations to answer this question. We disclosed some difference between the effects of the Meissner currents and Abrikosov vortices on the intergrain medium, which is fairly a nontrivial fact, not quite consistent with Eq. (2). To discard the effects related to the "uniqueness" or "specificity" of the investigated sample, we carried out a series of magnetotransport measurements on different HTS samples. The results obtained on four HTS samples of the yttrium (YBCO) system with different critical transport current densities and somewhat different shapes of magnetic hysteresis loops allowed us to unambiguously state that the Meissner current (in grains) and trapped Abrikosov vortices (also in grains) can affect differently the field in the intergrain medium. An explanation for the discovered behavior was proposed.

The article is organized as follows. In Sect. 2, we briefly characterize the samples and describe the details of the magnetotransport and magnetization measurements. In Sect. 3, we provide evidence for the validity of considering an HTSs as a two-level superconductor (grains and grain boundaries), present the experimental R(H) dependences, and describe their features, which are well explained within the concept of an effective field in the intergrain medium (Eq. (2)). In addition, based on the magnetization and magnetoresistance data, we determine the field of the first penetration into grains. It is necessary to establish experimental conditions for the Meissner state of the HTSC grains. Next, we demonstrate the validity of the approach in which the condition $R = \text{const}$ for different branches of the hysteretic R(H) dependence can be used to analyze the magnetoresistance hysteresis. It should be noted, that Sect. 3 is kind of a brief review of the magnetotransport properties of granular HTSs, since the described features of the R(H) and M(H) dependences and their interplay are typical of such materials. In Sect. 4, we report on the comparison of the resistance (for the condition $R = \text{const}$) for the considered states: (**AV**) with the trapped flux and (**MC**) with the Meissner effect. The experiments were carried out on different samples under essentially different external conditions. In Sect. 5, we propose our interpretation of the result obtained, which consists in the features of orientation arrangement of the Abrikosov vortices and configuration of Meissner currents inside grains with the anisotropy of the superconducting properties. Section 6 contains the main conclusions made.

2 Brief Characterization of the Samples and Details of the Measurements of Their Magnetotransport and Magnetic Properties

The investigated HTS samples of the $YBa_2Cu_3O_{7-\sigma}$ (hereinafter, YBCO-1, YBCO-2, and YBCO-3) and $Y_{0.96}Pr_{0.04}Ba_2Cu_3O_{7-\sigma}$ (hereinafter, YBCO-4) compositions were obtained by the solid-state synthesis in air from the corresponding oxides with 3−4 intermediate grindings. For sample YBCO-1, special measures were provided to optimize the conditions of annealing at the final synthesis stage (about 50 h at a temperature 940 °C with subsequent exposure at 350 °C for 10 h). For the rest samples, such measures were not taken. The total annealing at the intermediate stages at temperatures of 910−930 °C lasted for about 100 h and, at the final stage, after cooling, an additional exposure in a furnace at 350 °C for 3−5 h was performed. The X-ray diffraction patterns of the synthesized samples contained only the reflections corresponding to the 1–2-3

structure. Table 1 gives the main parameters of the samples: critical temperature T_C (the onset of the resistive transitions), critical current density j_C at T = 77.4 K, resistivity ρ above the superconducting transition, physical density, and average grain size determined by scanning electron microscopy (Hitachi-TM 4000 microscope was used). The values listed in Table 1 are typical of granular HTSs with the 1–2-3 structure. It can be seen that sample YBCO-1 exhibits the best transport characteristics; a certain decrease in the T_C value for sample YBCO-4 is caused by praseodymium.

The magnetotransport properties, including the *I–V* characteristics and electrical resistance R, were measured by the four-probe method. The sample sizes varied within $0.4-1.2\times0.4-1.2\times4-9$ mm^3; parallelepiped samples were cut from the prepared tablets. The most of R(H) measurements or the *I–V* measurements aimed at determining the critical current I_C, which are analyzed in this work, were carried out on a sample placed in liquid nitrogen, which allowed us to use sufficiently large instrumental values of transport current I (up to 1 A for sample YBCO-1 for several hours) without thermal heating of the sample. An external field was specified by a copper solenoid immersed in liquid nitrogen (a stable field of up to 2 kOe), an electromagnet, or a superconducting solenoid. The external field variation rate dH/dt ranged from 0.5 to 8 Oe/s (these cases are discussed below) and the conventional dH/dt value was 1−2 Oe/s. The direction of the external field relative to the macroscopic transport current **I** (the long part of the sample) will be specified for each experiment; the parallel ($\mathbf{H} \parallel \mathbf{I}$) and perpendicular ($\mathbf{H} \perp \mathbf{I}$) configurations were used. When measuring the R(T) dependences, the sample was in the heat-exchange helium atmosphere (a part of the R(T) and R(H) measurements at a weak transport current was carried out on a Quantum Design PPMS-9 T Physical Property Measurement System). The critical current I_C was determined from the *I–V* characteristics using the voltage drop criterion (~10^{-6} V); the critical current was traced until $I_C > 1$ mA.

The magnetic measurements were carried out on an original vibrating sample magnetometer [45] and a Lake-Shore VSM 8604 magnetometer. To ensure the correct comparison of the magnetotransport data, the thermomagnetic prehistories of a sample should be completely identical. The magnetization and magnetotransport measurements were carried out on the same samples at the same mutual configuration of geometric sizes of the sample and the external field, including the dH/dt values.

Most of the analyzed magnetoresistance (critical current) and magnetization data were obtained at a temperature of 77.4 K. An exception is some of the R(H) isotherms presented in SubSect. 3.1 (Figs. 2b and 3b).

Table 1 Parameters of the investigated samples

Sample	T_C, K (onset)	j_C (77.4 K), A/cm^2	ρ (95 K), mΩ·cm	average grain size, μm	density, % theor
YBCO-1	93	150	0.45	10	93
YBCO-2	92.8	60	1.2	4	86
YBCO-3	92	40	1.5	5	85
YBCO-4	91	12	2.1	6	85

3 Concept of an Effective Field in the Intergrain Medium and Description of the Magnetoresistance Hysteresis

3.1 Manifestation of Two Superconducting Subsystems in the Magnetotransport and Magnetic Properties

To illustrate the concept of an effective field in the intergrain medium described in Introduction, we use the experimental results obtained on the investigated samples. First, we show in what external field and temperature ranges and in which subsystem (HTS grains or grain boundaries) the dissipation occurs. To do that, let us turn to the R(T) dependences in an external field shown in Figs. 2a and 3a for samples YBCO-1 and YBCO-3, respectively; in Figs. 2 and 3, the logarithmic scale along the *y* axis is used. The two-stage resistive transition clearly pronounced in Figs. 2a and 3a reflects the existence of two superconducting subsystems. A sharp decrease in the resistance with a decrease in temperature occurs, first, in grains; after that, the system of grain boundaries passes into the superconducting state. This is manifested especially clearly in fairly weak external fields, although the two-stage nature of the resistive transition can also be observed in fields of tens of kilooersted. In addition, it can be seen that the transition from the dissipation in intergrain boundaries to the dissipation in grains occurs at approximately the same resistance value. This value denoted as R_{NGB} is the normal resistance of the subsystem of grain boundaries (analogously to the Josephson terminology). Obviously, the total resistance of the sample at $T > T_C$ is

$$R_{tot} = R_{NGB} + R_{NG}, \tag{3}$$

where R_{NG} is the resistance of all superconducting grains and R_{tot} is the resistance of the entire sample at $T = T_C$. The R_{NGB}/R_{tot} ratio is a characteristic of a superconductor, which does not change when another parallelepiped cut out from a synthesized tablet is used. However, the R_{NGB}/R_{tot} values for the HTSs from different sets (in our case, YBCO-1, -2, -3, and -4) are different.

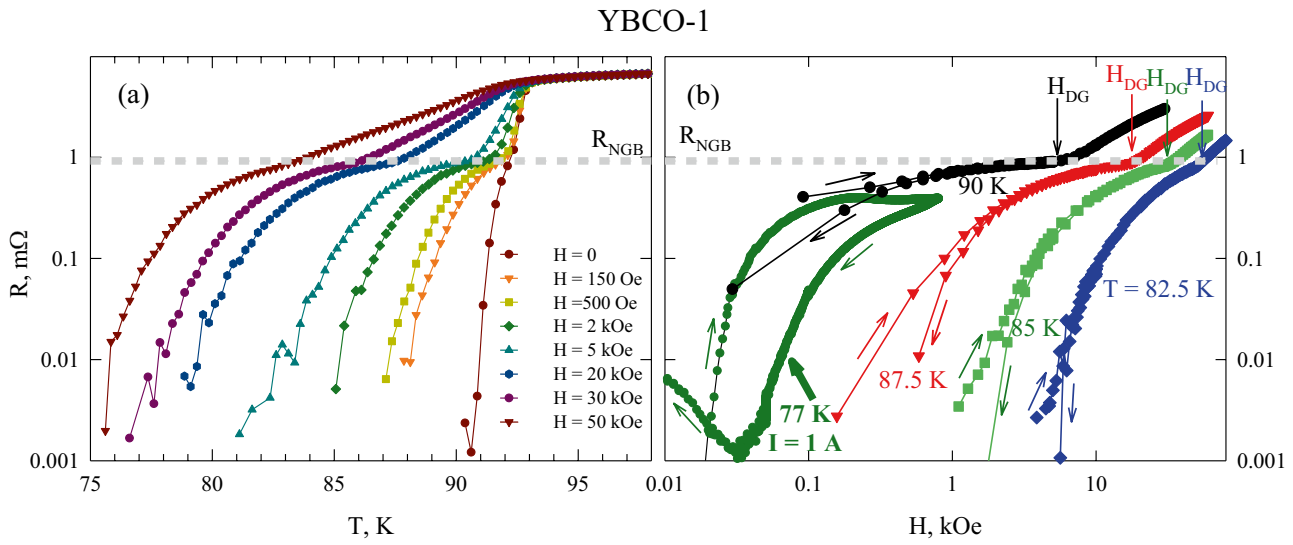

Fig. 2 **a** R(T) dependences in different external fields and **b** R(H) dependences at different temperatures for sample YBCO-1. The resistance axis is the logarithmic scale (in **a** and **b**). Horizontal dashed lines show the R_{NGB} value, i.e., the maximum magnetoresistance of the subsystem of grain boundaries. In **b**, the abscissa axis is the logarithmic scale and arrows show the external field variation direction. The external field corresponding to the onset of the dissipation in superconducting grains is denoted as H_{DG}. The current is I=1 mA for all data in **a** and **b**, except for those marked in **b** as I=1 A; here, the transport current is 1000 mA and the configuration **H** ∥ **I** is used. For the rest data, the configuration is **H** ⊥ **I**

The two-stage nature of the superconducting transition manifests itself also in the R(H) magnetoresistance isotherms shown in Figs. 2b and 3b. In these figures, the ordinate axes are the same as in Figs. 2a and 3a, i.e., the R(T) data in (a) and R(H) data in (b) can be compared; the abscissa axis in Figs. 2b and 3b is the logarithmic scale. Figures 2b and 3b show the general trend to an increase in the resistance with the external field with an intermediate plateau in the R(H) dependences at a resistance level of $R = R_{NGB}$ followed by another growth of the R(H) dependence. Equation (3) can be rewritten as

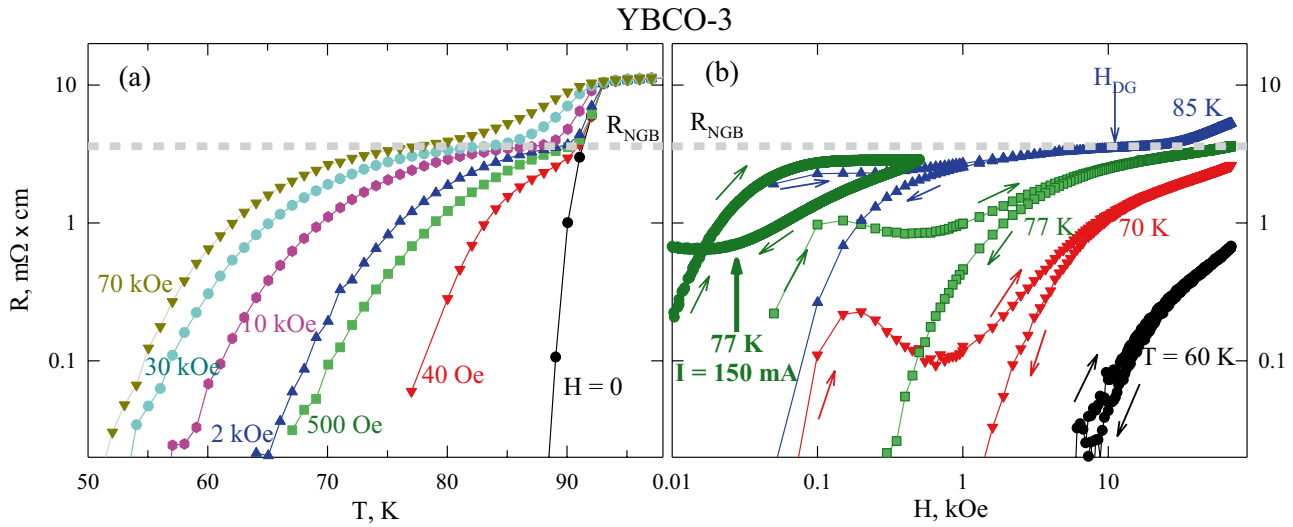

Fig. 3 **a** R(T) dependences in different external fields and **b** R(H) dependences at different temperatures for sample YBCO-3. The resistance axis is the logarithmic scale (in **a** and **b**). Horizontal dashed lines show the R_{NGB} value, i.e., the maximum magnetoresistance of the subsystem of grain boundaries. In **b**, the abscissa axis is the logarithmic scale and arrows show the external field variation direction. The external field corresponding to the onset of the dissipation in superconducting grains is indicated as H_{DG}. The current is I=2 mA for all data in **a** and **b**, except for those marked in **b** as I=150 mA. The configuration **H** ∥ **I** is used. For the rest data, the configuration is **H** ⊥ **I**

$$R(H) = R_{GB}(H) + R_G(H), \quad (4)$$

where $R_{GB}(H)$ is the magnetoresistance of the subsystem of grain boundaries and $R_G(H)$ is the magnetoresistance of HTS grains. First, the magnetoresistance growth is caused by the dissipation in grain boundaries, i.e., only the first term of Eq. (4) works, saturating at $R_{GB}(H = H_{DG}) = R_{NGB}$ (dashed horizontal lines in Figs. 2 and 3); with a further increase in the field, at $H \geq H_{DG}$, the dissipation in superconducting grains begins (the second term of Eq. (4) starts working). Here, H_{DG} is the field corresponding to the onset of the dissipation in grains (see Figs. 2b, 3b) accompanied by a change in the R(H) curvature sign (at $H = H_{DG}$). As can be seen in Figs. 2 and 3, at a temperature of 77.4 K, the dissipation in grains can only begin at a sufficiently large (above 50–60 kOe) H_{DG} value. In this case, a multiple increase in the transport current does not lead to the dissipation in grains in this range, which is consistent with the results reported in [46]. This can be seen from the positioning of the R(H) dependences measured at I = 1 A (Fig. 2b) and I = 150 mA (Fig. 3b) and the horizontal lines $R = R_{NGB}$. In all the cases, we have $R < R_{NGB}$ (at $H < H_{DG}$).

Let us also pay attention to the shape of the R(H) dependences in the region of the dissipation in the intergrain medium (at $R < R_{NGB}$, the behavior of the first term in Eq. (4)). According to the data in Figs. 2b and 3b, the magnetoresistance exhibits hysteresis: the R value for an increasing external field is larger than that for a decreasing field. Sometimes, a local R(H) maximum is also observed when the field increases and an R(H) minimum is observed when the field decreases. If the transport current is weaker than the critical current, then the state with R = 0 will be implemented instead of the minimum. After decrease the external field to zero, the sample can show a remanent resistance (see the data obtained at I = 1A in Fig. 2b and at I = 150 mA in Fig. 3b). The R(H) hysteresis exists in the field region below $H = H_{DG}$ (Figs. 2b and 3b), i.e., before the onset of the dissipation in grains. The R(H) and $I_C(H)$ measurements analyzed below were carried out down to the fields significantly lower than H_{DG} at a temperature of 77 K; it can be stated with confidence that the dissipation occurs entirely in the subsystem of grain boundaries.

Let us consider the R(H) hysteresis under inversion of the external field. A typical example is presented in the inset in Fig. 4. Here, one should distinguish between the initial magnetoresistance curve $R(H_{ini})$ obtained after cooling in zero field and the magnetoresistance branches for decreasing (H_{dec}) and increasing (H_{inc}) fields (indicated in the inset in Fig. 4). The state with the remanent magnetoresistance R_{Rem} is implemented at $H_{dec} = 0$ and, at the same values of the maximum applied field $H_{inc} = \pm H_{max}$, the R(H) dependence is symmetric with respect to the *y* axis. The above-mentioned nonmonotonic behavior of the

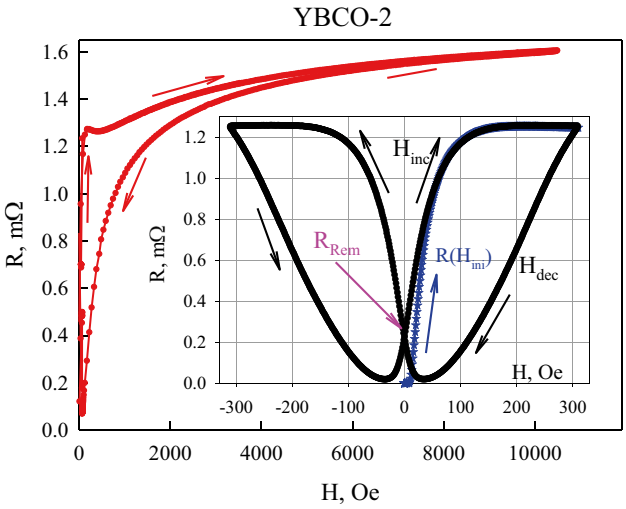

Fig. 4 Hysteretic R(H) dependence for sample YBCO-2; the current is I = 300 mA (T = 77.4 K, configuration $\mathbf{H} \perp \mathbf{I}$). Inset: initial $R(H_{ini})$ curve and R(H) hysteresis loop upon field cycling to $H_{max} = \pm 310$ Oe. The designations H_{ini} for the initial field, H_{inc} for the increasing field, H_{dec} for the decreasing field, and R_{Rem} for the remanent magnetoresistance are given. Arrows show the external field variation direction

$R(H_{inc})$ (or $R(H_{ini})$) dependence appears usually in fields of $H_{inc} \sim 100-200$ Oe at a temperature of 77 K and can be clearly identified by considering a much wider external field range, as shown for the R(H) dependence in Fig. 4 (the $R(H_{inc})$ maximum is pronounced).

To describe the magnetoresistance hysteresis within the concept of an effective field in the intergrain medium, the behavior of the magnetic hysteresis should be traced. Figure 5 shows the M(H) dependences for the investigated samples. The data presented in Fig. 5 illustrate the interplay between the initial $M(H_{ini})$ curve and $M(H_{inc})$ and $M(H_{dec})$ branches upon field cycling to a certain H_{max} value; the inset in Fig. 5a illustrates the effect of the field variation rate dH/dt on the shape of the M(H) curve. The inset in Fig. 5b shows a series of M(H) loops obtained upon field cycling to different H_{max} values.

Considering the data shown in the inset in Fig. 5b, we should pay attention to the lesser M(H) hysteresis in the range of up to ± 8 Oe. A similar hysteresis was observed previously in [47, 48]. This is obviously a response from the subsystem of grain boundaries; in addition, in this field range, the magnetic field in a granular superconductor is completely screened. The penetration of the magnetic field into grains occurs in a somewhat stronger field and the field value corresponding to the first penetration can be found either as the field at which the M(H) dependence deviates from the linear dependence [49–51] or from the $M_{Rem}(H_{max})$ behavior. Figure 6 presents the $M_{Rem}(H_{max})$ dependences for samples YBCO-1 and YBCO-2. At sufficiently high H_{max} values (400−500 Oe), the $M_{Rem}(H_{max})$ dependence saturates; then,

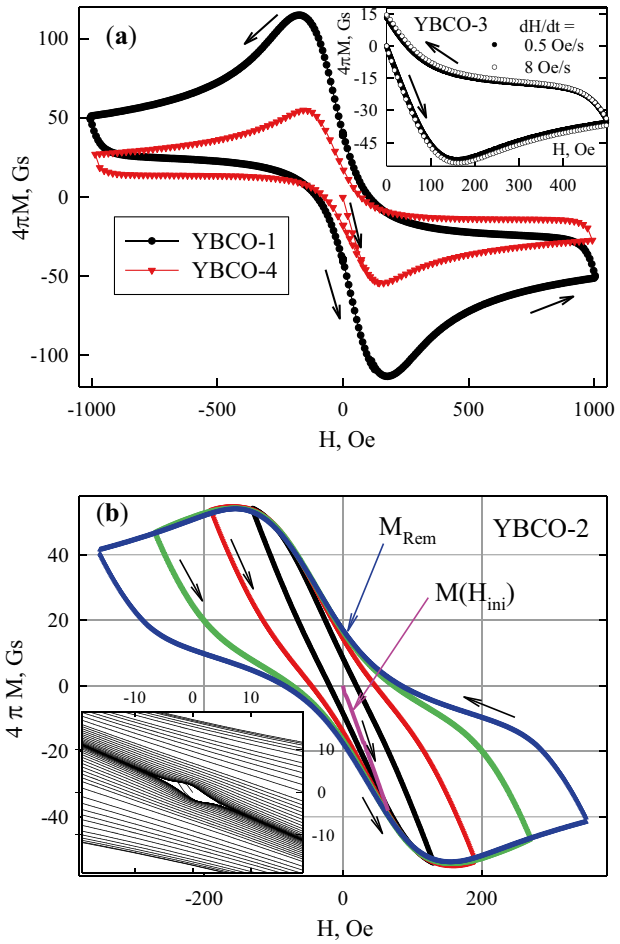

Fig. 5 M(H) dependences for the investigated samples at T = 77.4 K. The initial magnetization curve $M(H_{ini})$ and the M(H) curve upon field cycling, as well as the remanent magnetization M_{Rem} are shown. Inset in **a** effect of the field variation rate dH/dt on the M(H) curve (sample YBCO-3). Inset in **b** partial magnetic hysteresis loops upon field cycling to different H_{max} values (3−400 Oe). Arrows show the external field variation direction

we can speak about the "closed" magnetic hysteresis loop (by analogy with ferromagnets). In weak (several Oersted) fields, there is the contribution of the subsystem of grain boundaries (the lesser hysteresis in the inset in Fig. 5b); therefore, the $M_{Rem}(H_{max})$ dependence starts not with zero, but with some M_{Rem} value. As can be seen in the inset in Fig. 6, the $M_{Rem}(H_{max})$ dependence deviates from a constant value in fields of 35–40 Oe, and the indicated field H_{C1G} is the first penetration field for the superconducting grains.

Interestingly, the lesser magnetic hysteresis (inset in Fig. 5b) does not appear in the magnetoresistance, and the R(H) hysteresis appears starting with the field H_{C1G}, according to Eq. (2). This is demonstrated for the samples YBCO-2 и YBCO-3 in Fig. 7a, b, where the R(H) dependences, which were obtained by changing the field to different maximum values and then decreasing to zero, are presented. The red ovals in Fig. 7 mark the H_{max} value, which is the nearly limiting value for reversible magnetoresistance behavior. The marked value of H_{max} for sample YBCO-2 (Fig. 7a) is about 35 Oe. This result agrees with H_{C1G} value obtained from the magnetization data (inset in Fig. 6). For sample YBCO-3 irreversible behavior starts, also, from H ≈ 35 Oe. So, we conclude that the Meissner state realizes in the superconducting grains of YBCO-1, YBCO-2, and YBCO-3 at H < 35 Oe and T = 77.4 K (for zero field cooling regime).

3.2 Description of the R(H) Hysteresis and its Properties

Now, let us turn to an example of the description of the magnetoresistance hysteresis in terms of the concept of an effective field in the intergrain medium, see subsection 1.1. Figure 8a shows the R(H) dependences for sample YBCO-2 obtained by cycling the external field to different H_{max} values. As formula (2) demonstrates, there is a direct correspondence between the magnetization hysteresis loop M(H) and the magnetoresistance hysteresis R(H) (meaning $R = f(B_{eff})$, see subSect. 1.1). It is suggested, that the same values of resistance $R(H_{dec})$ and $R(H_{inc})$ for the decreasing and increasing external magnetic fields mean the same values of the effective fields $B_{eff}(H_{dec})$ and $B_{eff}(H_{inc})$ in the intergrain medium [9, 13–15]. The magnetoresistance hysteresis width is determined as $\Delta H_R = H_{dec} - H_{inc}$ at $R(H_{dec}) = R(H_{inc})$; the effective field hysteresis width is determined similarly: $\Delta H_{Beff} = H_{dec} - H_{inc}$ at $B_{eff}(H_{dec}) = B_{eff}(H_{inc})$. The validity of formula (2) requires $\Delta H_R(H_{dec}) = \Delta H_{Beff}(H_{dec})$.

Figure 8b shows the $B_{eff}(H)$ dependences calculated using (2) from the M(H) dependences obtained on the same sample and under the same experimental conditions (Fig. 5b). It

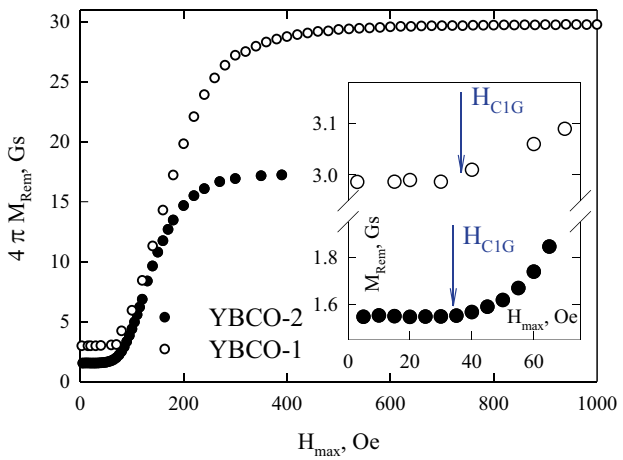

Fig. 6 H_{max} dependences of remanent magnetization M_{Rem} for samples YBCO-1 and YBCO-2 (T = 77.4 K). Inset: deviation of M_{Rem} from a constant value in the vicinity of the field H_{C1G} corresponding to the first penetration into grains

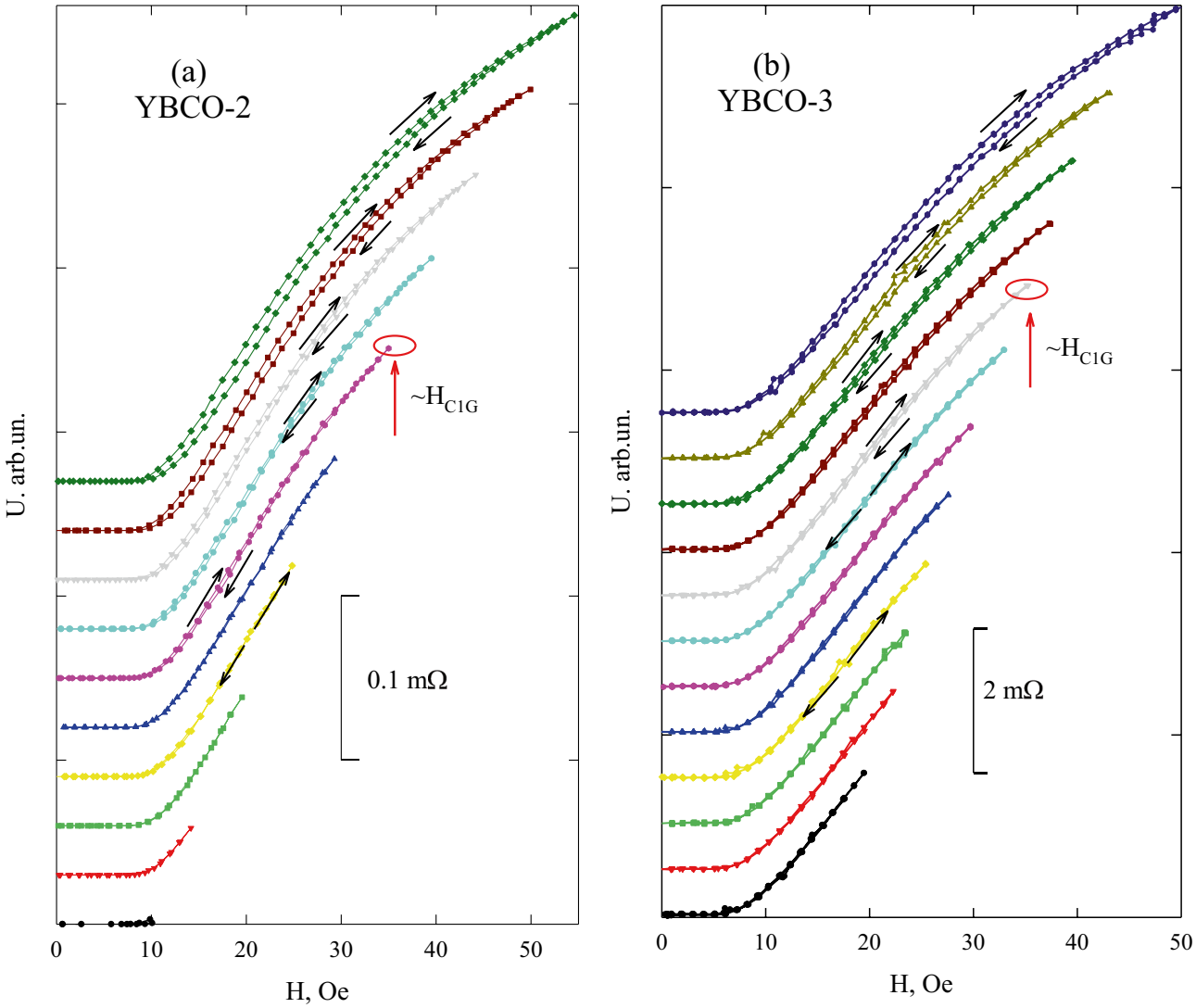

Fig. 7 Field dependences of the resistance of samples YBCO-2 (**a**) and YBCO-3 (**b**) with different (increasing) maximum external fields (I = 180 mA, T = 77.4 K, configuration **H** ∥ **I**). The data are given in mV (U = R · I) and shifted by a constant value along the *y* axis. The oval marks the dependence that starts demonstrating the irreversibility (hysteresis) due to attaining the field H_{C1G} corresponding to the first penetration into HTS grains. Arrows show the external field variation direction

is seen, that the R(H) and B_{eff}(H) dependences correlate. The local maximum appears on both the R(H_{inc}) and B_{eff}(H_{inc}) dependences. The local minimum, whose position shifts towards bigger external fields with increasing H_{max}, is also present on both the R(H_{dec}) and B_{eff}(H_{dec}) dependences. Both the experimental value of the remanent resistance R_{Rem} and the value of B_{eff} at $H_{dec} = 0$ growth with increasing H_{max}. The correlated behavior of the two dependences is achieved only for sufficiently large values of α. The B_{eff}(H) dependences in Fig. 8b were calculated at $\alpha = 22$. It should be noted that using the values of α out of $\alpha = 22 \pm 4$ breaks the correlations between the R(H) and B_{eff}(H) dependences. Functional dependences of $\Delta H_R(H_{dec})$ and $\Delta H_{Beff}(H_{dec})$ were discussed in works [13–15], and sufficiently large values of α were established for polycrystalline YBCO.

The R(H) dependences in Fig. 8a were obtained in the configuration **H** ⊥ **I**. At the parallel configuration (**H** ∥ **I**), the α value is somewhat smaller: $\alpha \approx 12$ (see [21, 22] for more detail). The large α value is, in fact, the manifestation of the magnetic flux compression in the intergrain medium (see Fig. 1) and the effective field in the intergrain medium can significantly (by more than an order of magnitude) exceed the external field H induced by a solenoid (see the data in Fig. 8b) [13–15].

The horizontal lines between thick symbols in Fig. 8a demonstrate the magnetoresistance hysteresis width ΔH_R

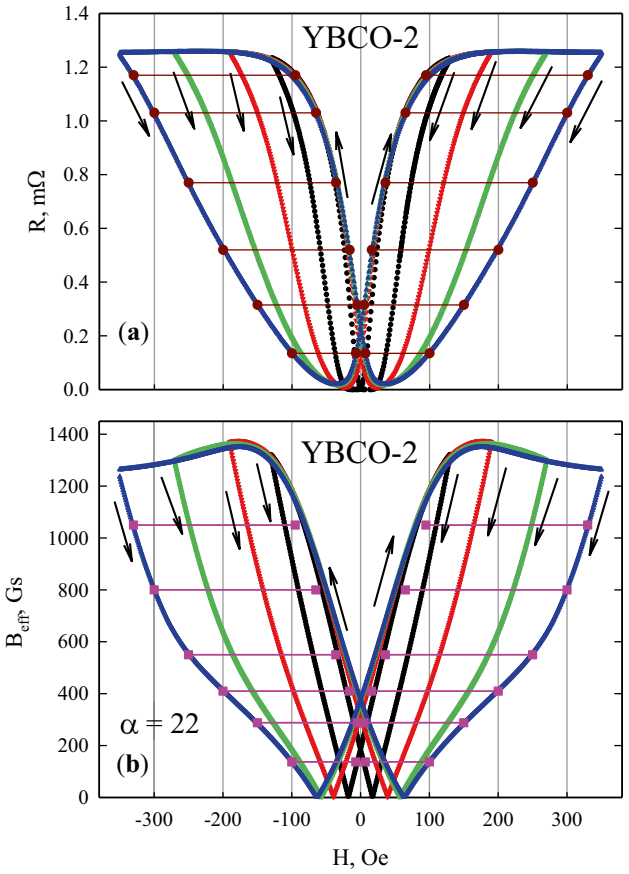

Fig. 8 **a** R(H) dependences (T = 77.4 K, configuration **H** ⊥ **I**) for sample YBCO-2 at different maximum fields H_{max} and **b** $B_{eff}(H)$ dependences calculated using Eq. (2) (from the magnetization data in Fig. 5b) at α = 22. The H axis is the same for these two graphs. The horizontal segments explain the meaning of the field width of the magnetoresistance hysteresis and the effective field (see the text). Arrows show the external field variation direction

at $H_{dec} = \pm 100, \pm 150, \pm 200, \pm 250, \pm 300, \pm 330$ Oe for $H_{max} = \pm 350$ Oe. The same horizontal segments are plotted in Fig. 8b. It is seen that some thick symbols for H_{inc} do not lie accurately on the $B_{eff}(H_{inc})$ branches, i.e. $\Delta H_R < \Delta H_{Beff}$. It means that some assumptions of the considered conception of the effective field (subsection 1.2) are not completely valid here. We suspect that the different effects of the trapped Abrikosov vortices and the Meissner currents are responsible for this mismatch.

To sum up this section, we illustrate one more peculiarity in the behavior of the magnetoresistance of granular HTSs. Above, we operated with the widths of the R(H) hysteresis (ΔH_R) and the $B_{eff}(H)$ hysteresis (ΔH_{Beff}). The effective field hysteresis width ΔH_{Beff} is determined by the magnetization of superconducting grains, which follows from Eq. (2); however, it would seem that the transport current should affect the magnetoresistance hysteresis width. Nevertheless, although the resistance is a nonlinear

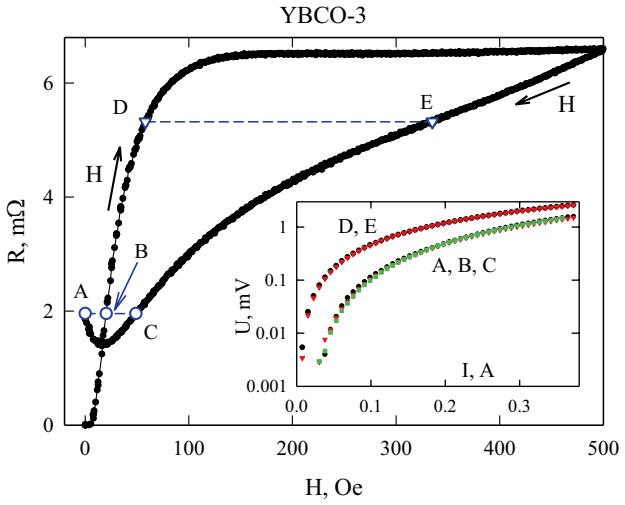

Fig. 9 Hysteretic R(H) dependence for sample YBCO-3 (T = 77.4 K, I = 150 mA, configuration **H** ∥ **I**); points A, B, C and D, E in the initial and descending R(H) branches are indicated at which the *I–V* characteristics shown in the inset were measured (in the inset, the logarithmic scale along the ordinate axis is used)

function of the current (i.e., the *I–V* characteristics are nonlinear), it turns out that the parameter ΔH_R almost does not depend on I. This was discovered and discussed in [9, 14, 16, 26]. In this work, we illustrate this property by the example of the *I–V* characteristics for sample YBCO-3 (inset in Fig. 9). Figure 9 shows the R(H) dependence and points in the $R(H_{ini})$ and $R(H_{dec})$ dependences in which we have $R(H_{ini}) = R(H_{dec})$ (points A, B, C and D, E). At I = 150 mA, in the indicated triple (A, B, C) and pair (D, E) of points, the resistance is the same. In this case, the *I–V* characteristics almost coincide at these points (inset in Fig. 9). Hence, we have $R_A = R_B = R_C$ and $R_D = R_E$ at any current and the hysteresis width $\Delta H_R = H_{dec} - H_{ini}$ is independent of the transport current, including the case of the remanent resistance (point A, $H_{dec} = 0$).

4 Comparison of the Meissner State and the Trapped Flux State

4.1 Formulation of the Conditions For Comparing the Remanent Resistance and the Resistance in the Initial Magnetoresistance Curve

As mentioned in Introduction, the main objective of this work was to compare the magnetoresistances for (**MC**) the Meissner state (the Abrikosov vortices have not yet penetrated into grains) and (**AV**) the trapped flux (in zero field in the remanent magnetization state). The data obtained in the previous section provide the prerequisites for such a comparison. First, the state with a trapped flux without

contribution of the Meissner currents is obtained if the maximum applied field is stronger than the field corresponding to the first penetration into grains ($H_{max} > H_{C1G} \approx 35$ Oe). Varying the H_{max} value, different remanent magnetizations M_{Rem} and, consequently, different amounts of the trapped flux can be obtained. The Meissner state is implemented under the conditions of the initial magnetization (and magnetoresistance) curve at $H_{ini} \equiv H^* < H_{C1G} \approx 35$ Oe, where H^* is the H_{ini} value providing $R(H_{ini} \equiv H^*) = R(H_{dec} = 0) = R_{Rem}$. These conditions (for a temperature of 77.4 K) were met in the experiments described below (SubSects. 4.2, 4.3, 4.4 and 4.5), while the H^* value was no higher than 30 Oe. Since the condition $R_{Rem} = R(H_{ini} = H^*)$ is equivalent to $B_{eff\_Rem} = B_{eff}(H_{ini} = H^*)$, we obtain from Eq. (2):

$$\alpha\, 4\pi \cdot M_{Rem} = H^* - \alpha \cdot 4\pi \cdot M\left(H_{ini} = H^*\right). \tag{5}$$

Therefore, to verify Eq. (5), we should find the experimental H^*, M_{Rem}, and $M(H^*)$ values from the condition $R_{Rem} = R(H_{ini} \equiv H^*)$ and corresponding magnetization data and obtain the α value. Looking ahead, we note that there is no agreement within Eq. (5); therefore, it is reasonable to separate the parameter α into the parameters α_{AV} and α_{MC}. Here, subscripts AV and MC correspond to the Abrikosov vortices and Meissner currents, respectively. Then, Eq. (5) will be rewritten in the form

$$\alpha_{AV} \cdot 4\pi \cdot M_{Rem} = H^* - \alpha_{MC} \cdot 4\pi \cdot M\left(H_{ini} = H^*\right). \tag{6}$$

Below, four methods for the analysis with Eq. (6) are proposed. These are (i) matching R_{Rem} to $R(H_{ini} \equiv H^*)$ and comparison of R_{Rem} after some time (relaxation effects), (ii) matching R_{Rem} and $R(H_{ini} \equiv H^*)$ for different amounts of the trapped flux, (iii) matching R_{Rem} and $R(H_{ini} \equiv H^*)$ for the R(H) dependences measured at the essentially different field variation rates dH/dt, and (iv) comparison of the critical currents I_{C_Rem} at $H_{dec} = 0$ and I_C in the increasing external field $H = H_{ini} \equiv H^*$.

4.2 Condition $R_{Rem} = R(H_{ini})$ Before and After Relaxation of the Remanent Resistance and Magnetization

Figure 10a shows the low-field portion of the hysteretic R(H) dependence for sample YBCO-1 (the H axis is the lower scale). This sample, which is characterized by a high critical current density (see Table 1), needs a strong transport current (I = 1 A) to observe the remanent resistance R_{Rem} and its relaxation $R_{Rem}(t)$ over time. The total R(H) hysteresis is presented in Fig. 2b (the maximum applied field H_{max} is 800 Oe). In addition, Fig. 10a shows the $R_{Rem}(t)$ dependence (the logarithmic time axis is the upper scale and the R axis is the same for the R(H) data and R(t) data).

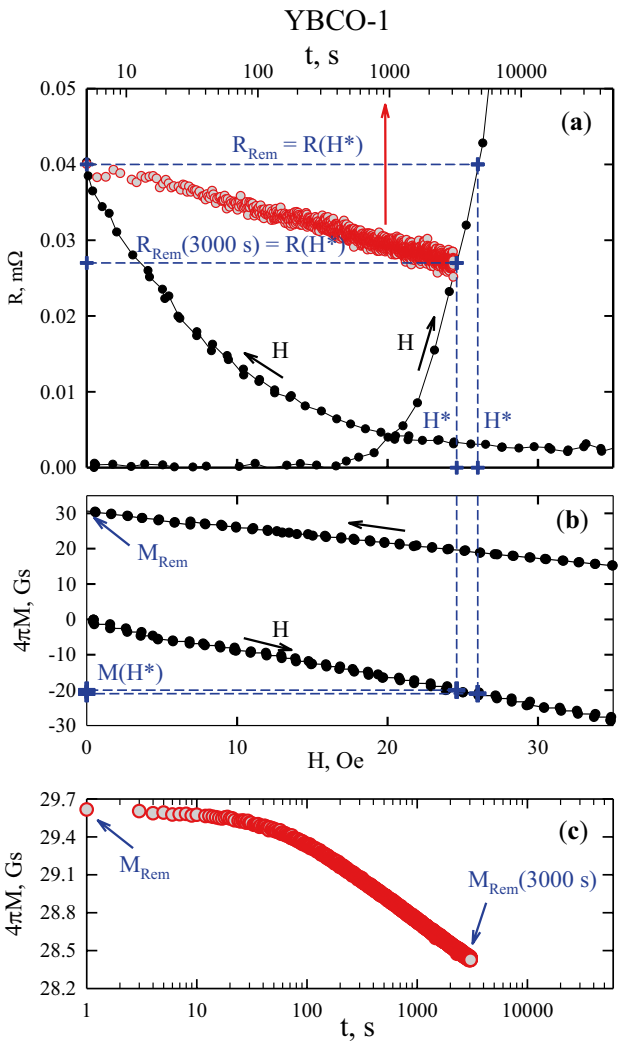

Fig. 10 Low-field portions of **a** the R(H) dependence (the current is I = 1 A, H_{max} = 800 Oe) and **b** M(H) dependence for sample YBCO-1. In (a), the abscissa (H) axis is the lower scale similar to the scale in **b**. In **a**, the time dependence of the remanent resistance (the time axis on the top is the logarithmic scale) is also shown; the R ordinate axis is the same for the R(H) and R(t) data. Horizontal dotted lines illustrate the conditions $R_{Rem}(t=0) = R(H_{ini} = H^*)$ and $R_{Rem}(t = 3000\ s) = R(H_{ini} = H^*)$. Vertical dotted lines show the determination of H^* and $M(H_{ini} = H^*)$ (for **b**). **c** Relaxation of the remanent magnetization $M_{Rem}(t)$ and a value of $M_{Rem}(t = 3000\ s)$ is indicated. The t axis scale is logarithmic

It can be seen that, over a time of t = 3000 s, the remanent resistance drops by about a third of its value.

Within the concept of effective field in the intergrain media, the change of the effective field results in the change of resistance. In our case the decrease of resistance is due to the relaxation of magnetization. The relaxation of the remanent magnetization $M_{Rem}(t)$ is shown in Fig. 10c. Generally, the magnetization relaxation in II type superconductors is attributed to thermally activated motion of Abrikosov vortices [25]. The character of relaxation and the relaxation rate

depend on external field, thermomagnetic prehistory, and temperature [25]. In our case $H = H_{dec} = 0$, and, the magnetization relaxation is related to the exit of the Abrikosov vortices from grains. Given $H_{dec} = 0$, formula (2) can be written as

$$B_{eff_{Rem}}(t) \equiv B_{eff}(H = 0, t) = \left|-\alpha_{AV} \cdot 4\pi \cdot M_{Rem}(t)\right|.$$

In Fig. 10a, one can see how the H* values, at which the equalities $R_{Rem}(t = 0) = R(H_{ini} = H^*)$ and $R_{Rem}(t = 3000\ s) = R(H_{ini} = H^*)$ are valid, can be determined for the $R(H_{ini})$ dependence. At the same time, the M values meeting the equality $M(H_{ini} = H^*)$ can be found from the data in Fig. 10b (in Figs. 10a, b, the abscissa (H) axis is the same). The M_{Rem} value is determined from Fig. 10b (or Fig. 10c) and, using the data from Fig. 10c, the $M_{Rem}(t = 3000\ s)$ value can be determined. The obtained experimental values of the magnetization and field H* (given in Table 2) cannot ensure the equality defined by Eq. (5). On the other hand, the successive substitution of these values into Eq. (6) yields the following relations between α_{MC} and α_{AV}:

$$\alpha_{MC} = 1.41 \cdot \alpha_{AV} - 1.24 \text{ for } t = 0,$$

$$\alpha_{MC} = 1.42 \cdot \alpha_{AV} - 1.23 \text{ for } t = 3000\ s.$$

Thus, approximately the same ratio between the quantities α_{AV} and α_{MC} is obtained both before and after the relaxation. The parameters α_{AV} and α_{MC} separately cannot be found. However, taking into account that the parameter α in itself (and, consequently, the parameters α_{AM} and α_{MC}) is always larger than 10 (see SubSect. 3.2), we unambiguously obtain $\alpha_{MC} > \alpha_{AV}$.

4.3 Condition $R_{Rem} = R(H_{ini})$ at Different Trapped Fluxes (Different H_{max} Values)

In the previous subsection, the maximum applied field H_{max} was 800 Oe; in this case, we can say that the magnetization hysteresis loop is closed and a further increase in H_{max} does not lead to the M_{Rem} growth (see Fig. 6). Therefore, it is reasonable to compare R_{Rem} and $R(H_{ini})$ when M_{Rem} takes intermediate values. In fact, in this case, it is necessary to study the R(H) hysteresis at different H_{max} values. Then, each H_{max} value will correspond to different amount trapped flux (at $H_{dec} = 0$).

Figure 11a shows the low-field portions of the selected hysteretic R(H) dependences ($R(H_{ini})$ and $R(H_{dec})$) for sample YBCO-2 at the H_{max} values indicated in the figure legend. Here, the transport current is 300 mA; some R(H) dependences in a wider H range are presented in Figs. 4 and 8a. Using the data from Fig. 11a, under the condition $R_{Rem} = R(H_{ini} = H^*)$, one can find the H* values corresponding to different H_{max} values. Next, the $M(H_{ini} = H^*)$ and M_{Rem} values can be found from the initial $M(H_{ini})$ curve (Fig. 11b) and a set of the data on the M(H) hysteresis loops measured to different H_{max} values. Fifteen sets of values in total were analyzed for fifteen different H_{max} quantities at which R_{Rem} and $R(H_{ini})$ can be compared. Some of these

Table 2 Methods for comparing the conditions of the Meissner state and the state with a trapped flux; parameter values and experimental conditions M_{Rem}, H*, and M(H*) values obtained from the analysis of the data presented in Figs. 10, 11, 12, and 14; and relations between α_{MA} and α_{AV} obtained from them using Eq. (6)

Sample, orientation, figure, and subsection	Method and conditions	H_{max}, Oe	$4\pi M_{Rem}$, Gs	H*, Oe	$4\pi M(H^*)$, Gs	Relation between α_{MC} and α_{AV}	Result (at α_M, $\alpha_A > 10$)
YBCO-1	$R_{Rem} = R(H^*)$	800	29.6	26.0	−21.0	$\alpha_{MC} = 1.41\ \alpha_{AV} - 1.24$	$\alpha_{MC} > \alpha_{AV}$
H ∥ **I**	$R_{Rem}(t) = R(H^*)$	800	28.4	24.6	−20.0	$\alpha_{MC} = 1.42\ \alpha_{AV} - 1.23$	$\alpha_{MC} > \alpha_{AV}$
Fig. 10, Subsec. 4.2	(after relaxation)						
YBCO-2	$R_{Rem} = R(H^*)$						
H ⊥ **I**,		130	8.6	10	−5.8	$\alpha_{MC} = 1.48\ \alpha_{AV} - 1.72$	$\alpha_{MC} > \alpha_{AV}$
Fig. 11,	different H_{max}	190	14.2	15.3	−9.1	$\alpha_{MC} = 1.56\ \alpha_{AV} - 1.68$	$\alpha_{MC} > \alpha_{AV}$
Subsec. 4.3	(15 values)	270	16.7	18.1	−10.5	$\alpha_{MC} = 1.59\ \alpha_{AV} - 1.72$	$\alpha_{MC} > \alpha_{AV}$
		350	17.3	18.7	−11.0	$\alpha_{MC} = 1.57\ \alpha_{AV} - 1.70$	$\alpha_{MC} > \alpha_{AV}$
YBCO-3	$R_{Rem} = R(H^*)$						
H ∥ **I**	dH/dt = 0.5 Oe/s	500	13.5	19.0	−10.4	$\alpha_{MC} = 1.30\ \alpha_{AV} - 1.83$	$\alpha_{MC} > \alpha_{AV}$
Fig. 12,	dH/dt = 8 Oe/s	500	14.5	19.3	−11.7	$\alpha_{MC} = 1.24\ \alpha_{AV} - 1.64$	$\alpha_{MC} > \alpha_{AV}$
Subsec. 4.4							
YBCO-4	$R_{Rem} = R(H^*)$	1000	18.3	13.0	−7.7	$\alpha_{MC} = 2.36\ \alpha_{AV} - 1.7$	$\alpha_{MC} > \alpha_{AV}$
H ⊥ **I**,	$I_{C\_Rem} = I_C(H^*)$	1000	18.3	14	−8.4	$\alpha_{MC} = 2.2\ \alpha_{AV} - 1.7$	$\alpha_{MC} > \alpha_{AV}$
Fig. 14, Subsec. 4.5							

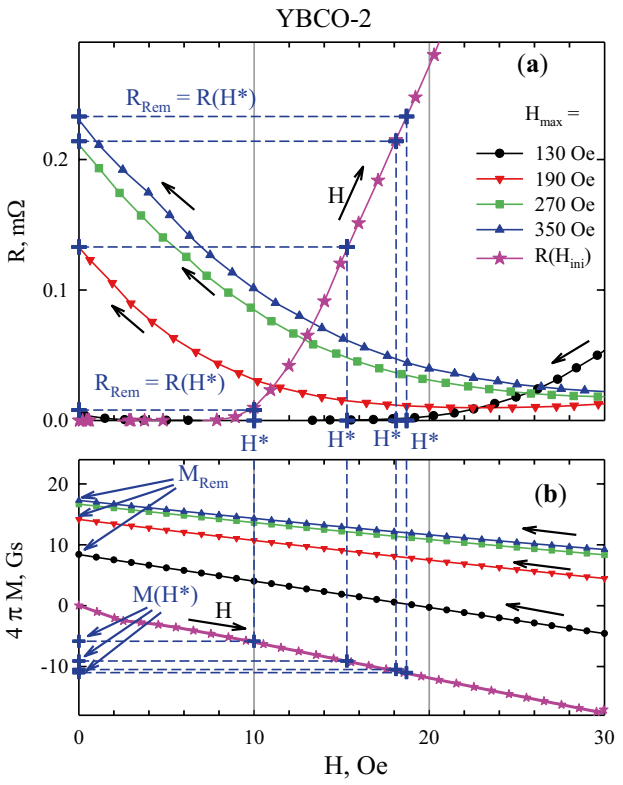

Fig. 11 Low-temperature portions of **a** the R(H) dependences (the current is I = 300 mA) at different H_{max} values and **b** similar M(H) dependences for sample YBCO-2. The H_{max} values indicated in the legend in **a**. In **a** and **b**, the abscissa (H) axes are the same. Horizontal dotted lines correspond to the condition $R_{Rem} = R(H_{ini} = H^*)$ and vertical dotted lines show the determination of H* and $M(H_{ini} = H^*)$ (for **b**)

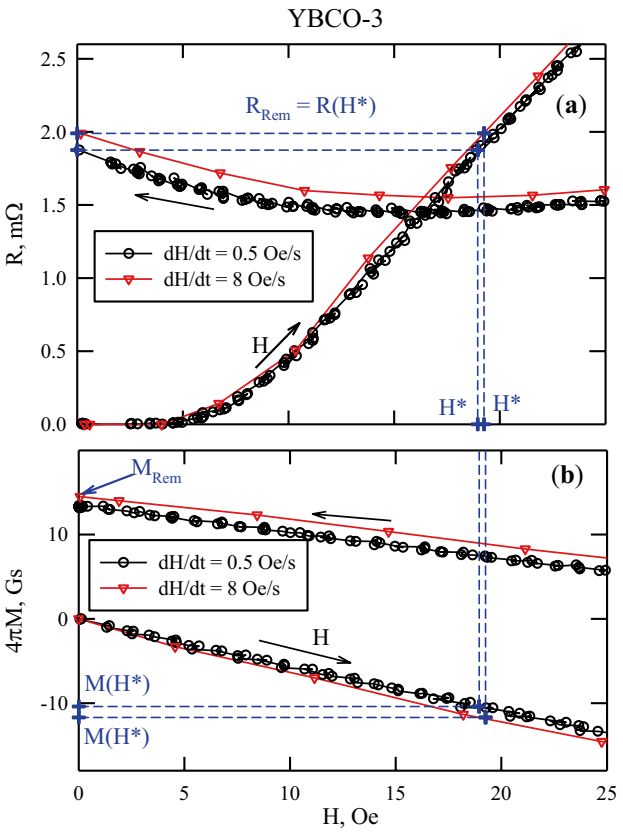

Fig. 12 Low-temperature portions of **a** the R(H) dependences (I = 150 mA and H_{max} = 500 Oe) measured at different field variation rates dH/dt (indicated in the legends) and **b** similar M(H) dependences for sample YBCO-3. In **a** and **b**, the abscissa (H) axes are the same. Horizontal dotted lines correspond to the condition $R_{Rem} = R(H_{ini} = H^*)$ and vertical dotted lines show how the H*, M_{Rem}, and $M(H_{ini} = H^*)$ were determined

values are given in Table 2. The four sets of the field H* and magnetization values from Table 2 are representative of all the data collected. As in the previous subsection, the relation between α_{MC} and α_{AV} (the penultimate column of Table 2) suggests $\alpha_{MC} > \alpha_{AV}$.

4.4 Condition $R_{Rem} = R(H_{ini})$ at Different Field Variation Rates dH/dt

A manifestation of the relaxation effects in the magnetic properties of type-II superconductors is the dependence of the magnetization hysteresis on the external field variation rate dH/dt. In this subsection, we consider the effect of relatively high and low magnetization switching rates on the results of comparison of R_{Rem} and $R(H_{ini})$. The dH/dt values were chosen to be 0.5 and 8 Oe/s. Figure 12a shows the low-field portions of the selected hysteretic R(H) dependences for sample YBCO-3 obtained at these rates. The maximum applied field for the data presented in Fig. 12a is 500 Oe, the transport current is I = 150 mA, and the R(H) dependence at an intermediate rate of dH/dt = 2 Oe/s is shown in Fig. 9.

The impact of different dH/dt values on the R_{Rem} values and the initial $R(H_{ini})$ curve can be seen in Fig. 12a. In this case, according to Fig. 12b, the field variation rate affects also the magnetization. The H*, $M(H_{ini} = H^*)$, and M_{Rem} values obtained by comparing R_{Rem} and $R(H_{ini})$ are given in Table 2. The ratio between α_{MC} and α_{AV} (the penultimate column of Table 2) unambiguously indicates the validity of the inequality $\alpha_{MC} > \alpha_{AV}$ for sample YBCO-3 at different dH/dt values.

4.5 Condition $I_{C\_Rem} = I_C(H_{ini})$

Above, we analyzed the resistance equality condition $R_{Rem} = R(H_{ini})$; in this case, according to the *I*–*V* characteristics (see the inset in Fig. 9), the transport current should not affect the results of the comparison. The R(H) measurements, including the remanent resistance R_{Rem}, suggest that the transport current exceeds the critical current I_C at any R(H) point. Nevertheless, it remains unanswered whether the resistance equality approach works when extended to

the critical current equality. To clarify this item, the R(H) dependence (at I = 350 mA) and the I_C(H) dependence (for it, it was necessary to switch-off the external field for the time of measuring the *I–V* characteristics (~1 s)) were measured. Figure 13 shows the R(H) dependence (the R axis is on the left) and the I_C(H) dependence (the I_C axis is on the right). It should be noted that the I_C(H) dependence can be seen in "the reasonably full scale" if a logarithmic scale is used along the I_C axis. The abscissa axis is a logarithmic scale as well. The I_C value in zero external field (without magnetic prehistory) is ~ 340 mA; then, as the field increases to ~ 40 Oe, the critical current decreases by more than two orders of magnitude (the critical currents weaker than 1 mA were not measured). However, the reverse $I_C(H_{dec})$ dependence ($H = H_{dec}$) exhibits constant nonzero values starting with $H_{dec} \approx 500$ Oe. There is a pronounced $I_C(H_{dec})$ maximum and the maximum field coincides with the field H_{dec} at which the $R(H_{dec})$ dependence has a minimum. In zero external field ($H_{dec} = 0$), the sample has a sufficient critical current I_{C_Rem}. We can state with a certain degree of conditionality that the I_C(H) dependence is a mirror image of the R(H) dependence.

Figure 14a shows the low-field portions of the hysteretic R(H) and I_C(H) dependences (for the data from Fig. 13) and, according to the conditions $R_{Rem} = R(H_{ini} = H^*)$ and $I_{C–Rem} = I_C(H_{ini} = H^*)$, provides examples of determining the H* values. Figure 14b presents examples of determining the $M(H_{ini} = H^*)$ and M_{Rem} values. We note that the values obtained from the comparison of the magnetoresistance and critical current are similar (Fig. 14 and Table 2). The relation between α_{MC} and α_{AV} (the penultimate column of Table 2) is consistent with the results for other samples (and approaches); it can also be concluded that the inequality $\alpha_{MC} > \alpha_{AV}$ is valid.

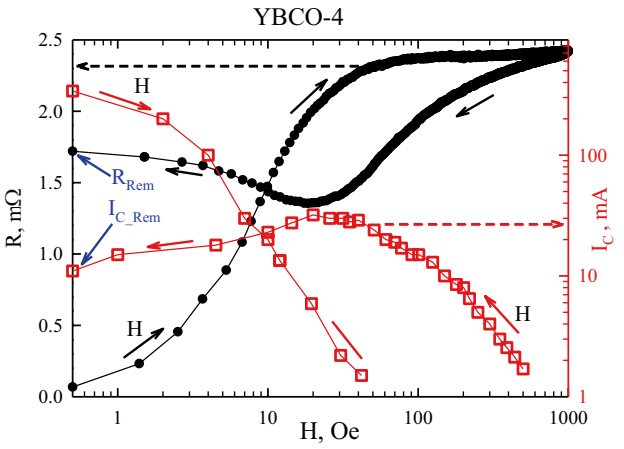

Fig. 13 Hysteretic R(H) dependence (the R axis is on the left) and I_C(H) dependence (the I_C axis is on the right (logarithmic scale)). The abscissa (H) axis is a logarithmic scale. For R(H), the transport current is I = 350 mA

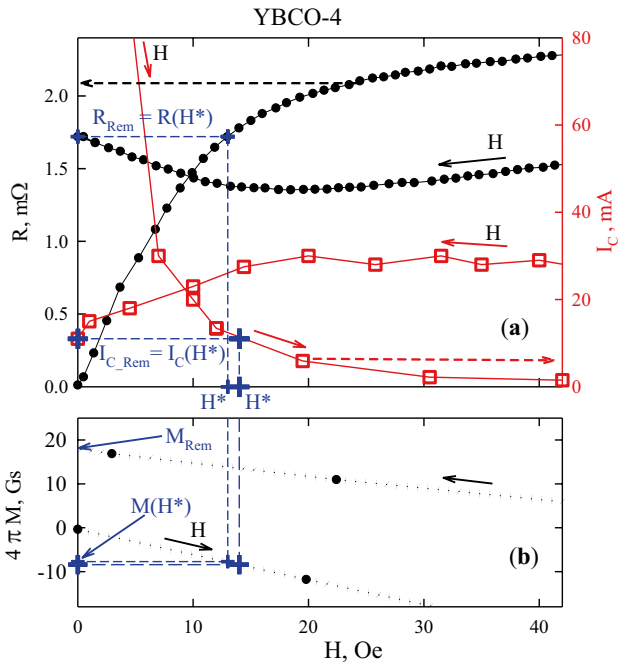

Fig. 14 Low-field portions of **a** the hysteretic R(H) dependence (the R axis is on the left) and I_C(H) dependence (the I_C axis is on the right) and **b** the M(H) dependence for sample YBCO-4. In **a** and **b**, the abscissa (H) axes are the same. (The R(H) and I_C(H) dependences for the entire field range are shown in Fig. 13). Horizontal dotted lines in **a** correspond to the conditions $R_{Rem} = R(H_{ini} = H^*)$ and $I_{C–Rem} = I_C(H_{ini} = H^*)$ and vertical dotted lines in **b** illustrate the determination of H*; in addition, the $M(H_{ini} = H^*)$ values are shown

5 Possible Reasons For the Different Effects of the Abrikosov Vortices and Meissner Currents on an Effective Field in the Intergrain Medium

The main result of Sect. 4 was the established invalidity of Eq. (5) and the experimentally confirmed validity of the inequality $\alpha_{MC} > \alpha_{AV}$ (following from Eq. (6)). In this section, we propose an interpretation of this result. In the schematic in Fig. 1, the vectors of the magnetic moments of grains are shown, which have projections of different signs onto the **Z** axis, depending on whether the external magnetic field increases or decreases. According to this, the value and sign of the magnetization changes (see Fig. 5). The magnetic response of a superconductor is formed from two contributions opposite in sign: magnetic moments $\mathbf{M}_M$ from the Meissner currents $\mathbf{I}_M$ and Abrikosov vortices $\mathbf{M}_{AV}$ (see the schematic in Fig. 15). The $\mathbf{M}_M$ and $\mathbf{M}_{AV}$ contributions to the field B_{eff} in the intergrain medium are also different in sign. In the two cases discussed here (only a trapped flux and only a Meissner state at $R_{Rem} = R(H_{ini} = H^*)$), the effective fields B_{eff_Rem} and $B_{eff}(H_{ini} = H^*)$ must have the same value, but different signs (Fig. 15). The result $\alpha_{MC} > \alpha_{AV}$ obtained in Sect. 4 means, however, that the Meissner currents and the

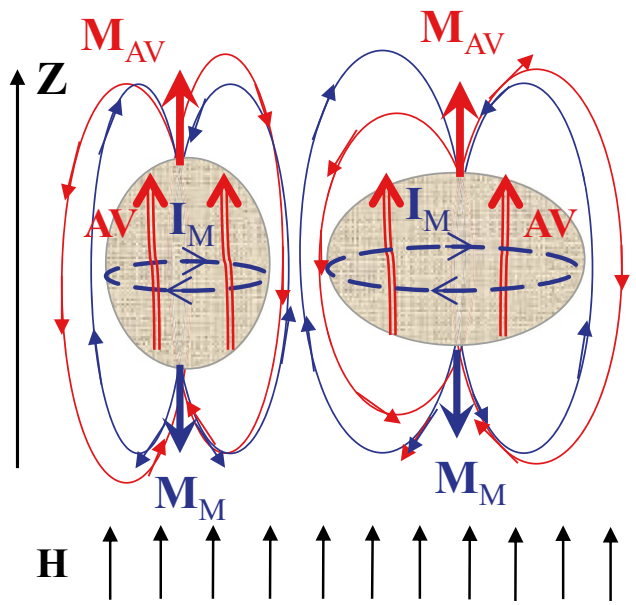

Fig. 15 Schematic of Meissner currents $\mathbf{I}_M$ and Abrikosov vortices **AV** in two adjacent superconducting grains (ovals) in an increasing external field. The space between grains is the grain boundary. M_M and M_{AV} are the magnetic moments created by the Meissner currents and Abrikosov vortices (from all vortices in one grain), respectively. Solid lines are lines of the magnetic induction M_M and M_{AV} from them (the directions are shown by arrows)

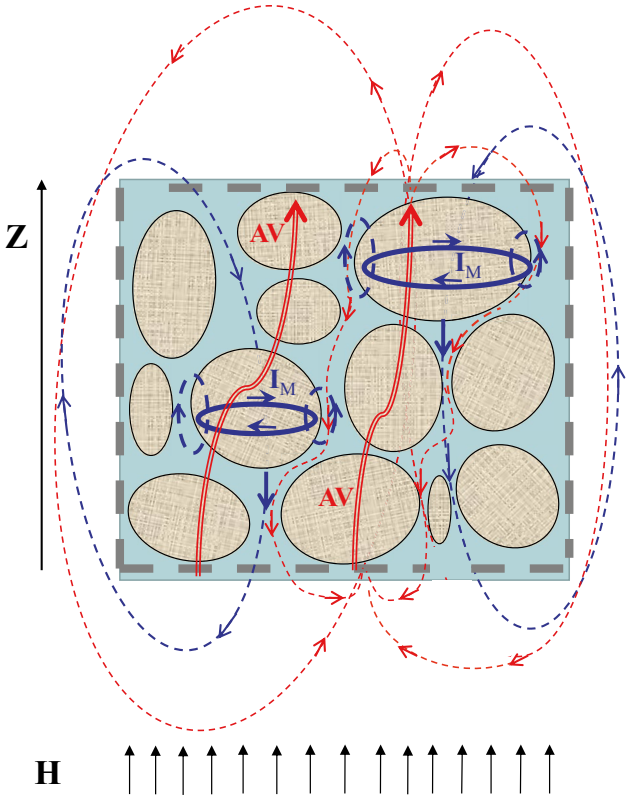

Fig. 16 Schematic of Meissner currents $\mathbf{I}_M$ and Abrikosov vortices **AV** in a granular superconductor of finite size (the square bounded by a dashed line). The ovals are grains and the space between them is the intergrain medium. The probable trajectories of the magnetic induction lines from the Abrikosov vortices and Meissner currents are shown

trapped flux affect differently the effective field in the intergrain medium. In other words, the "one-gauss" magnetization from the Meissner currents leads to a higher resistance in the intergrain medium than the "one-gauss" magnetization from the Abrikosov vortices. We find this result to be fairly nontrivial; it was obtained on different samples under different experimental conditions.

To explain the result obtained, it is reasonable to consider in more detail the positioning of the Abrikosov vortices and Meissner currents. The Abrikosov vortices in a granular HTS pierce many grains and exhibit the complex dynamics depending on field strength and temperature [25, 52, 53]. Within the critical state model, in zero external field (the remanent magnetization state), the vortices remain predominantly at the grain center [54]. The schematic in Fig. 16 illustrates the arrangement of vortices **AV** and Meissner currents $\mathbf{I}_M$, as well as the magnetic induction lines from them. There are the Meissner currents in all grains located both inside the sample and at its edge; the magnetic induction lines from them are closed both through the nearest intergrain spacings and outside the sample. The essential difference of the magnetic induction lines from the Abrikosov vortices is that the former start diverging at “one of the last” grains at the sample edge, rather than at each individual grain. The magnetic induction lines from the Abrikosov vortices should close both through the intergrain spacings and outside the sample. The latter, as for the magnetic induction lines from the Meissner currents, follows directly from the electromagnetism laws. Below, we offer an explanation of the discovered experimental fact $\alpha_{MC} > \alpha_{AV}$, considering the magnetic induction lines from the Abrikosov vortices and Meissner currents in the intergrain medium, taking into account the known anisotropy of the superconducting properties of HTS grains and the behavior of the Abrikosov vortices.

It is known well that the bismuth (BSCCO) HTS has the highest anisotropy of the critical current (and, consequently, of the diamagnetic signal) among HTS systems. However, for the yttrium HTS system, the ratio between the critical current densities along the *c* axis (J_{Cc}) and in the *ab* plane ($J_{Ca\text{-}b}$) is not at all low: $J_{Ca\text{-}b}/J_{Cc}$ ~4−8 [50, 55, 56]. In this case, the Meissner currents $I_{Ma\text{-}b}$ flowing in the *ab* plane exceed by far the Meissner currents I_{Mc} flowing in the planes parallel to the *c* axis [57, 58]. In an isotropic grain, the Meissner currents flow in the plane perpendicular to the external field and the Abrikosov vortices in a grain occupy the position predominantly parallel to the external field (|| **Z**), see Fig. 17a. In a grain with the anisotropic

superconducting properties, in the general case of the crystallographic *c* axis non-parallel to the axis **Z**, there are two diamagnetic contributions from the Meissner currents: $\mathbf{M}_{Mc}$ from the current $\mathbf{I}_{Ma\text{-}b}$ and $\mathbf{M}_{Ma\text{-}b}$ from the current $\mathbf{I}_{Mc}$ [57, 58], see Fig. 17b. In this case, the critical current ratio $J_{Ca\text{-}b}/J_{Cc} \sim 4-8$ leads to the fact that $\mathbf{M}_{Mc}$ exceeds by far (multiply) $\mathbf{M}_{Ma\text{-}b}$. The magnetization detected during the magnetic measurements is the sum of the projections $\mathbf{M}_{Mc}$ and $\mathbf{M}_{Ma\text{-}b}$ onto the **Z** axis: $M_{MZ} = M_{McZ} + M_{M\_a\text{-}b}$ (see Fig. 17b). Certainly, the resulting magnetization of a granular anisotropic superconductor is an averaged characteristic. However, it can be seen in Fig. 17b that the value of the magnetic moment $\mathbf{M}_{Mc}$ is larger than its projection onto the **Z** axis. It is clear that, in this case, the local effect of $\mathbf{M}_{Mc}$ on the intergrain medium will be stronger than expected from the M_{McZ} projection**.** Thus, the effect of the Meissner currents on the intergrain medium in anisotropic grains is expected to be somewhat stronger than can be assumed from the detected magnetization value.

The Abrikosov vortices inside anisotropic grains tend to orient along the *c* axis [1, 56], i.e., deviate from the external field direction. The question is in which direction the vortex magnetic induction lines exit a grain. If this direction coincides with the crystallographic *c* axis and a grain is considered "from the sample edge", then the magnetic moment $\mathbf{M}_{AV}$ from the Abrikosov vortex will be parallel to the *c* axis. In the schematic in Fig. 17b, this is indicated by (iii). In this case, the projection $\mathbf{M}_{AV}$ onto the **Z** axis (M_{AVZ}) will be smaller than $|\mathbf{M}_{AV}|$. Then, similarly to the Meissner currents, the effect of the magnetic moments from the Abrikosov vortices on the intergrain medium will be somewhat stronger than expected from the detected magnetization value. Then, the equality $\alpha_{MC} = \alpha_{AV}$ should be valid, which contradicts the experiment. Therefore, it is worth considering another option for the exit of vortices from grains. If we assume that the plasticity of the vortex lattice or another factor leads to the fact that, at the grain surface, the vortex tends to align parallel to the external field, then the value of the magnetic moment $\mathbf{M}_{AV}$ from the vortex will be almost equal to its projection M_{AVZ}. ($|\mathbf{M}_{AV}| \approx M_{AVZ}$). In Fig. 17b, these cases are indicated by (i) and (ii). The foregoing provides a consistent explanation for the observed stronger effect of the Meissner currents on the field in the intergrain medium as compared with the Abrikosov vortices. One of the reasons for the alignment of the vortices along the field near the grain edge may be a decrease in the anisotropy of the superconducting properties at the surface; i.e., we possibly deal with the manifestation of the surface effect. For the Meissner

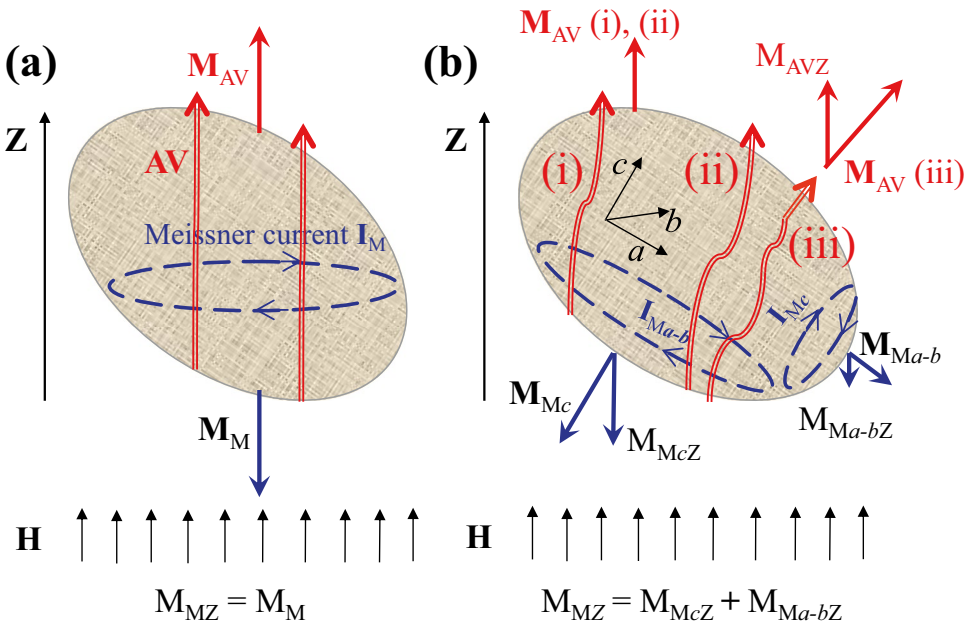

Fig. 17 Schematic of Meissner currents $\mathbf{I}_M$ and Abrikosov vortices **AV** in a superconducting grain (oval) in an increasing external field for a grain with **a** the isotropic and **b** anisotropic superconducting properties. In **a**, $\mathbf{M}_M$ and $\mathbf{M}_{AV}$ are the magnetic moments created by the Meissner currents and Abrikosov vortices, respectively. In **b**, the consideration typical of HTS is used, in which the anisotropy is determined by the crystallographic *ab* planes and the *c* axis with the ratio of the critical current densities $J_{Ca\text{-}b}/J_{Cc}$ much higher than unity. **b** Meissner currents $\mathbf{I}_{Ma\text{-}b}$ and $\mathbf{I}_{Mc}$ flowing in the *ab* planes and along the *c* axis, the magnetic moments $\mathbf{M}_{Mc}$ and $\mathbf{M}_{Ma\text{-}b}$ induced by these currents, and their projections M_{McZ} and $M_{Ma\text{-}bZ}$ onto the **Z** axis (**Z** ∥ **H**). The expressions for the projection of the total magnetic moment M_{MZ} from the Meissner currents onto the **Z** axis for the investigated cases are shown in the bottom. Projection M_{AVZ} of the magnetic moment $\mathbf{M}_{AV}$ onto the **Z** axis from the Abrikosov vortex will be $M_{AVZ} = M_{AV}$ for an isotropic grain **a** and for an anisotropic grain at vortex locations indicated by (i) and (ii) in **b**. The M_{AVZ} projection for vortex location (iii) is shown in **b**

currents, such a surface effect should be insignificant, since the field is screened for the entire intragrain space. Thus, the explanation proposed here for the different effects of the Meissner currents and Abrikosov vortices on the intergrain medium is based on the anisotropic properties of HTS grains and features of the vortex orientation inside them.

6 Concluding Remarks

The hysteresis of the magnetotransport properties (magnetoresistance and critical current) of granular HTSs is accompanied by quite a few intriguing features, most of which are adequately explained within the two-level superconductor model (a subsystem of grains and a subsystem of grain boundaries) and the concept of effective field B_{eff} in the intergrain medium of a granular superconductor. The relation between this effective field and the magnetic response from superconducting grains is given by Eq. (2), in which the parameter α is responsible for the magnetic flux compression in the intergrain medium.

In this study, using the example of the magnetic and magnetoresistive properties of several yttrium HTS samples, we illustrated the validity of considering two-level superconductors and demonstrated the validity of the concept of an effective field in the intergrain medium as applied to them. This part of the study is largely illustrative and has a form of a review, while further we considered in detail the dissipation (magnetoresistance and critical current) for two cases of the magnetic state of superconducting grains: the Meissner state (no flux trapping into grains) and the state with a trapped flux in zero external field. These states were compared according to the criterion of equality of the resistances ($R_{Rem} = R(H_{ini} = H^*)$) or the critical currents ($I_{C\_Rem} = I_C(H_{ini} = H^*)$). Such a comparison was made under different experimental conditions (variation of the maximum applied field and, consequently, the amount of the trapped flux, different external field variation rates dH/dt, account for the effect of relaxation of the remanent resistance and remanent magnetization). The main result obtained is the discovered difference between the effects of the Meissner currents and Abrikosov vortices on the intergrain medium. In other words, a "one-gauss" change in the magnetization from the Meissner currents makes a greater contribution to the effective field in the intergrain medium than a "one-gauss" change in the magnetization from the Abrikosov vortices. This is not quite consistent with Eq. (2) for the effective field, instead of which Eq. (6) ($\alpha_A \cdot 4\pi \cdot M_{Rem} = H^* - \alpha_M \cdot 4\pi \cdot M(H_{ini} = H^*)$) should be used. Here, the different effects of the Abrikosov vortices and Meissner currents are manifested in the fact that the corresponding parameters α_{MC} and α_{AV} are unequal and the inequality $\alpha_{MC} > \alpha_{AV}$ is valid.

The analysis of the reasons for the established fact allowed us to assume that the anisotropy of the superconducting properties of HTS grains (the YBCO systems) manifests itself differently for the Meissner currents and Abrikosov vortices. In the Meissner state, the dominant contribution is made by the currents circulating in the crystallographic *ab* planes; they induce a field into the intergrain medium, while the detected magnetic response is somewhat weaker. The Abrikosov vortices pierce many grains in a macroscopic HTS sample and tend to localize inside grains parallel to the crystallographic *c* axis. However, when the vortex leaves a grain at the sample edge, due to the surface effect, the direction of the magnetic induction lines from the vortex becomes such that, at the grain edge, the vortex tends to align parallel to the external field. In the described scenario, the effect of the vortices on the intergrain medium will be somewhat weaker than that of the Meissner currents, which, within the developed concept of an effective field in the intergrain medium, is expressed as $\alpha_{MC} > \alpha_{AV}$. The conclusion drawn can not only be used to explain the magnetoresistance hysteresis, but is also important for analyzing the magnetic properties of granular superconductors with the anisotropy.

Acknowledgements The authors are grateful to M.I. Petrov, A.D. Balaev, and V.M. Sosnin for fruitful discussions and A.V. Shabanov and I.V. Nemtsev for scanning electron microscopy investigations. The scanning electron microscopy investigations and a part of magnetic measurements (performed on a LakeShore VSM 8604 facility) were carried out at the Krasnoyarsk Regional Center for Collective Use, Krasnoyarsk Scientific Center, Siberian Branch of the Russian Academy of Sciences. The study is performed within the state assignment of Kirensky Institute of Physics.

Data Availability The data that support the findings of this study are available from the corresponding author upon reasonable request.

References

1. Blatter, G., Feigel'man, M.V., Gekshkebein, V.B., Larkin, A.I., Vinokur V.M.: Vortices in high-temperature superconductors. Rev. Mod. Phys. **66,** 1125 (1994). https://doi.org/10.1103/RevModPhys.66.1125
2. Eley, S., Glatz, A., Willa, R.: Challenges and transformative opportunities in superconductor vortex physics. J. Appl. Phys. **130**, 050901 (2021). https://doi.org/10.1063/5.0055611
3. Nattermann, T., Scheidl, S.: Vortex-glass phases in type-II superconductors. Adv. Phys. **49**(N5), 607–704 (2000). https://doi.org/10.1080/000187300412257
4. Huang, J., Wang, H.: Effective magnetic pinning schemes for enhanced superconducting property in high temperature superconductor $YBa_2Cu_3O_{7-x}$: a review. Supercond. Sci. Technol. **30**, 114004 (2017). https://doi.org/10.1088/1361-6668/aa8d32
5. Kwok, W.K., Welp, U., Glatz, A., Koshelev, A.E., Kihlstrom, K.J., Crabtree, G.W.: Vortices in high-performance high-temperature superconductors. Rep. Prog. Phys. **79,** 116501 (2016). https://doi.org/10.1088/0034-4885/79/11/116501
6. Ji, L., Rzchowski, M.S., Anand, N., Tinkham, M.: Magnetic-field-dependent surface resistance and two-level critical-state

model for granular superconductors. Phys. Rev. B **47**, 470 (1993). https://doi.org/10.1103/PhysRevB.47.470
7. Likharev, K.K.: Superconducting weak links. Rev. Mod. Phys. **51**, 101 (1979). https://doi.org/10.1103/RevModPhys.51.101
8. Daghero, D., Mazzetti, P., Stepanescu, A., Tura, P.: Electrical anisotropy in high-Tc granular superconductors in a magnetic field. Phys. Rev. B **66**, 11478 (2002). https://doi.org/10.1103/PhysRevB.66.184514
9. Balaev, D.A., Dubrovskii, A.A., Shaykhutdinov, K.A., Popkov, S.I., Gokhfeld, D.M., Gokhfeld, Yu.S., Petrov, M.I.: Mechanism of the hysteretic behavior of the magnetoresistance of granular HTSCs: The universal nature of the width of the magnetoresistance hysteresis loop. J. Exp. Theor. Phys. **108**, 241 (2009). https://doi.org/10.1134/S106377610902006X
10. Balaev, D.A., Popkov, S.I., Semenov, S.V., Bykov, A.A., Shaykhutdinov, K.A., Gokhfeld, D.M., Petrov, M.I.: Magnetoresistance hysteresis of bulk textured $Bi_{1.8}Pb_{0.3}Sr_{1.9}Ca_2Cu_3O_x$ + Ag ceramics and its anisotrop. Phys. C **470**,61 (2010). https://doi.org/10.1016/j.physc.2009.10.007
11. Balaev, D.A., Dubrovskii, A.A., Popkov, S.I., Shaikhutdinov, K.A., Petrov, M.I.: Relaxation of the Remanent Resistance of Granular HTSC Y-Ba–Cu–O + CuO Composites after Magnetic Field Treatment. Phys. Solid State **50**(6), 1014 (2008). https://doi.org/10.1134/S1063783408060036
12. Balaev, D.A., Dubrovskiy, A.A., Popkov, S.I., Shaikhutdinov, K.A., Mart'yanovc, O.N., Petrov, M.I.: Nonmonotonic Behavior of Magnetoresistance, $R(H)$ Hysteresis, and Low_Temperature Heat Capacity of the $BaPb_{0.75}Bi_{0.25}O_3$ Superconductor in a Magnetic Field: Possible Manifestations of Phase Separation. J Exp. Theor. Phys. **110**(4), 584–593 (2010)
13. Balaev, D.A., Popkov, S.I., Sabitova, E.I., Semenov, S.V., Shaykhutdinov, K.A., Shabanov, A.V., Petrov, M.I.: Compression of a magnetic flux in the intergrain medium of a $YBa_2Cu_3O_7$ granular superconductor from magnetic and magnetoresistive measurements. J. Appl. Phys. **110**,093918 (2011). https://doi.org/10.1063/1.3657775
14. Semenov, S.V., Balaev, D.A.: Temperature behavior of the magnetoresistance hysteresis in a granular high-temperature superconductor: Magnetic flux compression in the intergrain medium. Phys. C **550**, 19 (2018). https://doi.org/10.1016/j.physc.2018.04.005
15. Semenov, S.V., Balaev, D.A.: Magnetoresistance Hysteresis Evolution in the Granular Y-Ba–Cu–O High-Temperature Superconductor in a Wide Temperature Range. J. Supercond. Nov. Magn. **32**, 2409 (2019). https://doi.org/10.1007/s10948-019-5043-2
16. Semenov, S.V., Balaev, D.A.: Model of the Behavior of a Granular HTS in an External Magnetic Field: Temperature Evolution of the Magnetoresistance Hysteresis. Phys. Solid State **62**, 1136 (2020). https://doi.org/10.1134/S1063783420070239
17. Balaev, D.A., Semenov, S.V., Petrov, M.I.: Correlation Between Magnetoresistance and Magnetization Hysteresis in a Granular High-T_C Superconductor: Impact of Flux Compression in the Intergrain Medium. J. Supercond. Nov. Magn. **27**, 1425 (2014). https://doi.org/10.1007/s10948-014-2491-6
18. Semenov, S.V., Gokhfel'd, D.M., Terent'ev, K.Y., Balaev, D.A.: Mechanisms of the Magnetoresistance Hysteresis in a Granular HTS with the Paramagnetic Contribution by the Example of $HoBa_2Cu_3O_{7-\delta}$. Phys. Solid State **63**(N12), 1785–1794 (2021). https://doi.org/10.1134/S1063783421100334
19. Lopez, D., Decca, R., de la Cruz, F.: Anisotropic energy dissipation, flux flow and topological pinning in ceramic superconductors. Supercond. Sci. Technol. **5**, 276 (1992). https://doi.org/10.1088/0953-2048/5/1S/061
20. Balaev, D.A., Prus, A.G., Shaukhutdinov, K.A., Gokhfeld, D.M., Petrov, M.I.: Study of dependence upon the magnetic field and transport current of the magnetoresistive effect in YBCO-based bulk composites. Supercond. Sci. Technol. **20**, 495 (2007). https://doi.org/10.1088/0953-2048/20/6/002
21. Balaev, D.A., Semenov, S.V., Pochekutov, M.A.: Anisotropy of the magnetoresistance hysteresis in the granular superconductor Y-Ba-Cu-O at different magnetic-field and transport-current orientations. J. Appl. Phys. **122**, 123902 (2017). https://doi.org/10.1063/1.4986253
22. Semenov, S.V., Balaev, D.A., Pochekutov, M.A., Velikanov, D.A.: Anisotropy of the Magnetoresistive Properties of Granular High-Temperature Superconductors Resulting from Magnetic Flux Compression in the Intergrain Medium, Physics of the Solid State, **59**. No. **7**, 1291 (2017). https://doi.org/10.1134/S1063783417070241
23. Balaev, D.A., Popkov, S.I., Semenov, S.V., Bykov, A.A., Sabitova, E.I., Dubrovskiy, A.A., Shaikhutdinov, K.A., Petrov, M.I.: Contributions from Inter-grain Boundaries to the Magneto-resistive Effect in Polycrystalline High-TC Superconductors. The Underlying Reason of Different Behavior for YBCO and BSCCO Systems. J. Supercond. Nov. Magn. **24**, 2129 (2011). https://doi.org/10.1007/s10948-011-1166-9
24. Balaev, D.A., Bykov, A.A., Semenov, S.V., Popkov, S.I., Dubrovskii, A.A., Shaykhutdinov, K.A., Petrov, M.I.: General regularities of magnetoresistive effects in the polycrystalline yttrium and bismuth high-temperature superconductor systems. Phys. Solid State **53**, 922 (2011). https://doi.org/10.1134/S1063783411050052
25. Yeshurun, Y., Malozemoff, A.P., Shaulov, A.: Magnetic relaxation in high-temperature superconductors. Rev. Mod. Phys. **68**, 911 (1996). https://doi.org/10.1103/RevModPhys.68.911
26. Semenov, S.V., Balaev, A.D., Balaev, D.A.: Dissipation in granular high-temperature superconductors: New approach to describing the magnetoresistance hysteresis and the resistive transition in external magnetic fields. J. Appl. Phys. **125**, 033903 (2019). https://doi.org/10.1063/1.5066602
27. Balaev, D.A., Semenov, S.V., Petrov, M.I.: Dominant Influence of the Compression Effect of a Magnetic Flux in the Intergranular Medium of a Granular High-Temperature Superconductor on Dissipation Processes in an External Magnetic Field. Phys. Solid State **55**, 2422 (2013). https://doi.org/10.1134/S1063783413120044
28. Olutas, M., Kilic, A., Kilic, K., Altinkok, A.: Irreversibility Effects and Low Field Magnetovoltage Measurements in Superconducting MgB_2 Near the Critical Temperature *Tc*. J. Supercond. Nov. Magn. **26**, 3369–3390 (2013). https://doi.org/10.1007/s10948-013-2201-9
29. Altinkok, A., Kilic, K., Olutas, M., Kilic, A.: Magnetovoltage Measurements and Hysteresis Effects in Polycrystalline Superconducting $Y_1Ba_2Cu_3O_{7-x}$ /Ag in Weak Magnetic Fields. J. Supercond. Nov. Magn. **26**, 3085 (2013). https://doi.org/10.1007/s10948-013-2139-y
30. Palau, A., Puig, T., Obradors, X., Pardo, E., Navau, C., Sanchez, A., Usoskin, A., Freyhardt, H.C., Fernández, L., Holzapfel, B., Feenstra, R.: Simultaneous inductive determination of grain and intergrain critical current densities of $YBa_2Cu_3O_{7-x}$ coated conductors. Appl. Phys. Lett. **84**, 230 (2004). https://doi.org/10.1063/1.1639940
31. Pratima, S.: Vats, Study of Thermally Activated Phase-Slip and Scaling of Magneto-Resistance Near TC in $YBa_2Cu_3O_{7-\delta}$/Ag bulk composites. J. Supercond. Nov. Magn. **35**, 2275–2283 (2022). https://doi.org/10.1007/s10948-022-06206-8
32. Olutas, M., Kilic, A., Kilic, K., Altinkok, A.: Flux motion and isotropic effects in MgB_2 near the critical temperature. Eur. Phys. J. B **85**, 382 (2012). https://doi.org/10.1140/epjb/e2012-30509-0
33. Barzola-Quiquia, J., Dusari, S., Chiliotte, C., Esquinazi, P.: Andreev Reflection and Granular Superconductivity Features Observed in Mesoscopic Samples Using Amorphous Tungsten

Carbide Superconductors. J. Supercond. Nov. Magn. **24**, 463–469 (2011). https://doi.org/10.1007/s10948-010-0973-8
34. Bykov, A.A., Terent'ev, K.Y., Gokhfeld, D.M., Savitskaya, N.E., Popkov, S.I., Petrov, M.I.: Superconductivity on interfaces of nonsuperconducting granules La_2CuO_4 and $La_{1.56}Sr_{0.44}CuO_4$. J. Supercond. Nov. Magn. **31**, 3867–3874 (2018). https://doi.org/10.1007/s10948-018-4668-x
35. Derevyanko, V.V., Sukhareva, T.V., Finkel, V.A.: Magnetoresistance hysteresis of granular $YBa_2Cu_3O_{7-\delta}$ high-temperature superconductor in weak magnetic fields. Tech. Phys. **53**, 321 (2008). https://doi.org/10.1134/S1063784208030067
36. Sukhareva, T.V., Finkel, V.A.: Hysteresis of the magnetoresistance of granular HTSC $YBa_2Cu_3O_{7-\delta}$ in weak fields. Phys. Solid State **50**, 1001 (2008). https://doi.org/10.1134/S1063783408060012
37. Balaev, D.A., Semenov, S.V., Gokhfeld, D.M.: New Evidence of Interaction Between Grain and Boundaries Subsystems in Granular High-Temperature Superconductors. J. Supercond. Nov. Magn. **34**, 1067–1075 (2021). https://doi.org/10.1007/s10948-021-05812-2
38. Derevyanko, V.V., Sungurov, M.S., Sukhareva, T.V., Finkel', V.A., Shakhov, Y.N.: Phase Transitions in a MgB_2 Granular BCS Superconductor in Weak Magnetic Fields. Phys. Solid State **59**, 229–235 (2017). https://doi.org/10.1134/S1063783417020056
39. Zhu, X., Yang, H., Fang, L., Mu, G., Wen, H.H.: Upper critical field, Hall effect and magnetoresistance in the iron-based layered superconductor $LaFeAsO_{0.9}F_{0.1-\delta}$. Supercond. Sci. Technol. **21**, 105001 (2008). https://doi.org/10.1088/0953-2048/21/10/105001
40. Shaikhutdinov, K.A., Balaev, D.A., Popkov, S.I., Petrov, M.I.: Thermally activated dissipation in a novel foamed Bi-based oxide superconductor in magnetic fields. Supercond. Sci. Technol. **20**, 491 (2007). https://doi.org/10.1088/0953-2048/20/6/001
41. Gokhfeld, D.M., Balaev, D.A., Semenov, S.V., Petrov, M.I.: Magnetoresistance Anisotropy and Scaling in Textured High-Temperature Superconductor $Bi_{1.8}Pb_{0.3}Sr_{1.9}Ca_2Cu_3O_x$. Phys. Solid State, **57**(N11), 2145–2150 (2015). https://doi.org/10.1134/S1063783415110128
42. Eremets, M.I., Minkov, V.S., Drozdov, A.P., Kong, P.P., Ksenofontov, V., Shylin, S.I., Bud'ko, S.L., Prozorov, R., Balakirev, F.F., Sun, D., Mozaffari, S.: High-Temperature Superconductivity in Hydrides. J. Supercond. Nov. Magn. **35**, 965–977 (2022). https://doi.org/10.1007/s10948-022-06148-1
43. Troyan, I.A., Semenok, D.V., Kvashnin, A.G., Sadakov, A.V., Sobolevskiy, O.A., Pudalov, V.M., Ivanova, A.G., Prakapenka, V.B., Greenberg, E., Gavriliuk, A.G., Lyubutin, I.S.: Anomalous high-temperature superconductivity in YH6. Adv. Mater. , 2006832 (2021). https://doi.org/10.1002/adma.202006832
44. Hirsh, J.E.: Granular Superconductivity in Hydrides Under Pressure. J. Supercond. Nov. Magn. **35**, 2731–2736 (2022). https://doi.org/10.1007/s10948-022-06340-3
45. Balaev, A.D., Boyarshinov, Yu.V., Karpenko, M.M., Khrustalev, B.P.: Automated Superconductive-Solenoid Magnetometer. Prib. Tekh. Eksp. **3**, 167 (1985)
46. Prester, M.: Current transfer and initial dissipation in high-Tc superconductors. Supercond. Sci. Technol. **11**, 333–357 (1998). https://doi.org/10.1088/0953-2048/11/4/002
47. Jung, J., Mohamed, M.K., Cheng, S.C., Franck, J.P.: Flux motion, proximity effect, and critical current density in $YBa_2Cu_3O_{7-\delta}$/silver composites. Phys. Rev. B **42**, 6181–6195 (1990). https://doi.org/10.1103/PhysRevB.42.6181
48. Andrzejewski, B., Guilmeau, E., Simon, C.: Modelling of the magnetic behavior of random granular superconductors by the single junction model. Supercond. Sci. Technol. **14**, 904–909 (2001). https://doi.org/10.1088/0953-2048/14/11/304
49. Böhmer, C., Brandstätter, G., Weber, H.W.: The lower critical field of high-temperature superconductors. Supercond. Sci. Technol. **10**, A1–A10 (1997). https://doi.org/10.1088/0953-2048/10/7A/002
50. Liang, R., Dosanjh, P., Bonn, D.A., Hardy, W.N., Berlinsky, A.J.: Lower critical fields in an ellipsoid-shaped $YBa_2Cu_3O_{6.95}$ single crystal. Phys. Rev. B **50**(N7), 4212–4215 (1994). https://doi.org/10.1103/PhysRevB.50.4212
51. Pérez, F., Obradors, X., Fontcuberta, J., Bozec, X., Fert, A.: Magnetic flux penetration and creep in a ceramic (Y, Sm)$Ba_2Cu_3O_7$ superconductor. Supercond. Sci. Technol. **9**, 161–175 (1996). https://doi.org/10.1088/0953-2048/9/3/007
52. Koblischka, M.R., Naik, S.P.K., Koblischka-Veneva, A., Murakami, M., Gokhfeld, D., Reddy, E.S., Schmitz, G.J.: Superconducting YBCO Foams as Trapped Field Magnets. Materials **12**(6), 853 (2019). https://doi.org/10.3390/ma12060853
53. Koblischka, M.R., Naik, S.P.K., Koblischka-Veneva, A., Gokhfeld, D., Murakami, M.: Flux creep after field trapping in $YBa_2Cu_3O_x$ foams. Supercond. Sci. Technol. **33**(4), 044008 (2020). https://doi.org/10.1088/1361-6668/ab72c3
54. Bean, C.P.: Magnetization of high-field superconductors. Rev. Mod. Phys. **36**, 31–39 (1964). https://doi.org/10.1103/RevModPhys.36.31
55. Umezawa, A., Crabtree, G.W., Liu, J.Z., Moran, T.J., Malik, S.K., Nunez, L.H., Kwok, W.L., Sowers, C.H.: Anisotropy of the lower critical field, magnetic penetration depth, and equilibrium shielding Current in Single crystal $YBazCu_30_7$-δ. Phys. Rev. B **38**(N4), 2843–2846 (1988)
56. Bending, S.J., Dodgson, M.J.W.: Vortex chains in anisotropic superconductors. J. Phys. Condens. Matter **17**, R955–R993 (2005). https://doi.org/10.1088/0953-8984/17/35/R01
57. Gokhfeld, D.M., Balaev, D.A.: Magnetization Anisotropy in the Textured Bi-2223 HTS in Strong Magnetic Fields. Phys. Solid State **62**(7), 1145–1149 (2020). https://doi.org/10.1134/S1063783420070069
58. Gokhfeld, D.M., Semenov, S.V., Petrov, M.I., Nemtsev, I.V., Balaev, D.A.: Anisotropy and Crystallite Misalignment in Textured Superconductors. J. Supercond. Nov. Magn. **36**, 59–55 (2023). https://doi.org/10.1007/s10948-022-06454-8